ISTANBUL TECHNICAL UNIVERSITY ★ GRADUATE SCHOOL OF SCIENCE ENGINEERING AND TECHNOLOGY

PROCESSING AND INTERPRETATION OF BOOMER-SOURCED HIGH-RESOLUTION SHALLOW SEISMIC DATA ACQUIRED IN LAKE SAPANCA, TURKEY

M.Sc. THESIS

Gökçe İREGÖR

Department of Geophysical Engineering

Geophysical Engineering Programme

JUNE 2019

ISTANBUL TECHNICAL UNIVERSITY ★ GRADUATE SCHOOL OF SCIENCE ENGINEERING AND TECHNOLOGY

PROCESSING AND INTERPRETATION OF BOOMER-SOURCED HIGH-RESOLUTION SHALLOW SEISMIC DATA ACQUIRED IN LAKE SAPANCA, TURKEY

M.Sc. THESIS

Gökçe İREGÖR
(505151410)

Department of Geophysical Engineering

Geophysical Engineering Programme

Thesis Advisor: Prof. Dr. Hülya KURT

JUNE 2019

ISTANBUL TEKNİK ÜNİVERSİTESİ ★ FEN BİLİMLERİ ENSTİTÜSÜ

SAPANCA GÖLÜ'NE AİT BOOMER KAYNAKLI YÜKSEK ÇÖZÜNÜRLÜKLÜ SIĞ SİSMİK VERİLERİN İŞLENMESİ VE YORUMLANMASI

YÜKSEK LİSANS TEZİ

Gökçe İREGÖR
(505151410)

Jeofizik Mühendisliği Anabilim Dalı

Jeofizik Mühendisliği Programı

Tez Danışmanı: Prof. Dr. Hülya KURT

HAZİRAN 2019

Gökçe İregör, a M.Sc. student of İTU Graduate School of Science Engineering and Technology student ID 505151410, successfully defended the thesis entitled "Processing and Interpretation of Boomer-Sourced High-Resolution Shallow Seismic Data Acquired in Lake Sapanca, Turkey", which she prepared after fulfilling the requirements specified in the associated legislations, before the jury whose signatures are below.

Thesis Advisor :	**Prof. Dr. Hülya KURT** Istanbul Technical University	.....
Jury Members :	**Prof. Dr. Emin DEMİRBAĞ** Istanbul Technical University	.....
	Prof. Dr. Bedri ALPAR Istanbul University	.....

Date of Submission : 3 May 2019
Date of Defense : 13 June 2019

To all good souls,

FOREWORD

This thesis study was carried out using the data from TÜBİTAK-1001 (Project No: 117Y130) project titled "Active Tectonics Research of Lake Sapanca and Surroundings by Means of Geophysical Methods".

I would like to thank my advisor and mentor, Prof. Dr. Hülya KURT, for accepting me as one of her students, supporting me over the years during the MSc. studentship and making this thesis study possible.

Additionally, thanks to Geophysical Eng. MSc. N. Gözde OKUT TOKSOY for her advice on data processing and my classmates Geophysical Eng. Research Assistant Esra GÖNÜL and Geophysical Eng. Burak İNANÇ for their help, supportive discussions, valuable input and significant efforts during the data acquisition.

Thanks to the dean of Istanbul University Faculty of Aquatic Sciences, Prof. Dr. Meriç ALBAY for providing the research boat; SASKİ (Water and Sewerage Administration of Sakarya) for providing permission to use their pier; secretary of Istanbul University Faculty of Aquatic Sciences Vocational School of Higher Education, Mr. Bahattin KAYA for his help and support; captain of the boat, Harun UMUTLU and the employees of SONARSEA for their efforts during the data acquisition.

I would like to also thank my dear beloved husband and life partner, Tolga İREGÖR, for his everlasting support and understanding for everything and for being there.

April 2019

Gökçe İREGÖR
(Geophysical Engineer)

TABLE OF CONTENTS

Page

ABBREVIATIONS

AF : Antithetic fault
BP : Band-pass
CBF : Cross-basin fault
COS : Cosine
CTD : Conductivity, Temperature, Depth
GMT : The Generic Mapping Tools
HANN : Hanning
HAMM : Hamming
HP : High-pass
MF : Master fault
Min : Minimum
NAF : North Anatolian Fault
NAFZ : North Anatolian Fault Zone
RMS : Root-Mean-Square
SBP : Sub-bottom Profiling
SRTM : Shuttle Radar Topography Mission
TAU : Migration Layer Thickness
TRI : Triangular
TÜBİTAK : The Scientific and Technological Research Council of Turkey
TWT : Two-Way-Time
VD : Variable Density

SYMBOLS

A : Amplitude

c : Velocity of the Propagating Wavefield

f : Frequency

N : Number of Non-zero Samples

t : Zero-offset Two Way Travel Time

r : Wavefield Path Length

T : Sample Time

x : Distance

z : Depth of the Dipping Layer

β : Apparent Dip Angle

θ : True Dip Angle

LIST OF TABLES

Page

LIST OF FIGURES

Page

PROCESSING AND INTERPRETATION OF BOOMER-SOURCED HIGH-RESOLUTION SHALLOW SEISMIC DATA ACQUIRED IN LAKE SAPANCA, TURKEY

SUMMARY

This thesis study is carried out using the thirteen sub-bottom profiling lines (shallow seismic reflection profiles) and the bathymetry measurements acquired in the scope of TÜBİTAK-1001 project (Project No: 117Y130). The aim of the study is the application of common marine seismic data processing techniques on a Boomer-sourced, high-resolution shallow marine seismic reflection (Boomer sub-bottom profiling) data collected in Lake Sapanca, Turkey, the interpretation of the processed sections, and furthermore, to determine the characteristics of the active submarine tectonism in Lake Sapanca.

The study area Lake Sapanca is situated in the northwest Turkey between Izmit in the west and Sakarya in the east in the eastern Marmara region. Lake Sapanca is a freshwater basin created by faulting and is located on the northern strand of the western part of the North Anatolian Fault Zone (NAFZ) in a tectonically complex area which is well-reflected by the neighboring morphology consisting of a series of fault-generated mountain ranges defining the boundaries of the lake.

Tectonic regime in Turkey is ruled by three main elements; the Aegean-Cyprean Arc, the dextral North Anatolian Fault Zone and the sinistral East Anatolian Fault Zone. The Aegean-Cyprean Arc is a convergent plate boundary where the African Plate to the south is subducting beneath the Anatolian Plate to the north. The dextral North Anatolian Fault Zone and the sinistral East Anatolian Fault Zone are intracontinental strike-slip faults along which the Anatolian Plate moves westward away from the collision zone between the Arabian and the Eurasian plates. The North Anatolian Fault Zone (NAFZ) with its 1600 m length and dextral strike-slip characteristic is the most important element that governs the recent tectonic and morphologic development of the northern part of Turkey. The North Anatolian Fault Zone (NAFZ) is one of the most seismically active fault zones in the world which produces large magnitude earthquakes with mostly strike-slip displacements. The northern strand of NAFZ contains the segments which slipped during the 17 August 1999 Kocaeli earthquake of which the surface rupture passes through Lake Sapanca.

Previous researchers studying Lake Sapanca's submarine tectonic characteristics mainly describe Lake Sapanca as a pull-apart basin and the NAF yielding a pull-apart and/or step-over fault geometry.

Sub-bottom profiling (SBP) is a type of seismic reflection method which is used for shallow seismic reflection profiling operating at broader range of frequencies. Generation and detection of an acoustic wave is the common basic principle of the seismic reflection methods. Based on the same principle, in sub-bottom profiling, the source generates a short pulse of sound which travels through the water entering the seabed and the energy is reflected back from the boundaries between subsurface layers

of differing acoustic impedance. The reflected energy is sensed by a hydrophone or hydrophone array and recorded as a trace which then accumulated and displayed next to each other against time creating a profile. There are several types of sub-bottom profiling systems with various operating frequencies, resolution and penetration depths. The high-frequency "boomer" is one the most commonly used sub-bottom profilers providing high resolution and deep subsurface penetration. The Boomer source is an electromagnetically driven sound source which has been utilized as a marine seismic source for reflection surveys in deep and shallow waters. In the boomer, a heavy flow of current is discharged through a flat spiral coil inducing strong eddy currents in the aluminum front plate. Then the mutual repulsion pushes the front plate outward flexing away from the coils with high acceleration generating sound as this flexing creates an acoustic shock wave. The boomer source is usually mounted on a towed catamaran, which is towed behind a boat along with a separate single hydrophone or hydrophone array (streamer) as a receiver which are connected to a recording system onboard the towing vessel.

In this study, thirteen seismic reflection profiles were acquired in Lake Sapanca using a single-receiver, Boomer-sourced sub-bottom profiling method which is high-resolution and suitable for shallow waters. The length and the location of the lines were limited by the geographical features and practical aspects of the small boat operations. However, the lines were specifically chosen to be orientated north to south direction approximately perpendicular to the variations seen in the bathymetric data collected within the scope of the same TÜBİTAK-1001 project (117Y130).

Data processing was carried out in Nezihi Canıtez Data Processing Laboratory located in Department of Geophysical Engineering of Istanbul Technical University. Seismic data processing can be described as the manipulation of seismic data by means of computational techniques to obtain an enhanced image of the subsurface. Hence, data processing is important since correctly processed data leads to accurate interpretation of the subsurface structures. Since the survey area was relatively small and the acquired data characteristics were fairly similar, it was found suitable to use the same optimized parameters for every line. Data processing steps were, in the order of application, filtering, deconvolution, post-decon filtering, trace balancing and migration along with couple of mute applications prior to filtering and post-migration.

In the migrated seismic sections, the North Anatolian Fault reveals itself as a vertical discontinuity creating a small-scale folding on the lake bottom as well as sedimentary misalignments as it extends deeper. All discontinuities interpreted as the NAF can also be associated with the lineaments observed on the multibeam bathymetric image. Examining the fault map produced for this study, the NAF can be traced along Lake Sapanca as it enters from the south west corner of the lake and lengthens approximately 5 km towards the middle section of the lake with W-NW direction making an approximately 30˚ angle to the map plane. The fault slightly changes its direction towards the west as it continues almost straight for another 5 km until it leaves the lake at the north west corner. This fault geometry of the NAF indicates the fault has evolved with releasing bend characteristics in Lake Sapanca. Strike-slip-fault-like discontinuity observed in the southern part of the lake might be associated with the 22 July 1967 Mudurnu Valley earthquake surface rupture. The nature and the origin of another strike-slip-fault-like discontinuity seen on the southwest part of the lake is inconclusive due to no associations found on neighboring lines and also partly due to the lack of bathymetric data which could provide supportive evidence at the relevant location.

SAPANCA GÖLÜ'NE AİT BOOMER KAYNAKLI YÜKSEK ÇÖZÜNÜRLÜKLÜ SIĞ SİSMİK VERİLERİN İŞLENMESİ VE YORUMLANMASI

ÖZET

Bu tez çalışması 117Y130 no'lu TÜBİTAK-1001 Bilimsel Araştırma Projesi kapsamında Ağustos 2018'de Sapanca Gölü'nde toplanan 'boomer' kaynaklı sığ sismik yansıma verileri kullanılarak gerçekleştirilmiştir. Çalışmanın amacı, geleneksel sismik veri işlem aşamaları uygulanarak 'boomer' kaynaklı, yüksek çözünürlüklü sığ sismik yansıma verilerinin işlenmesi ve ardından yorumlanarak Sapanca Gölü'ne ait aktif teknonik özelliklerin belirlenmesidir.

Çalışma bölgesi olan Sapanca Gölü Türkiye'nin kuzeybatısında yeralan Marmara Bölgesi'nin doğusunda, batıda İzmit ve doğuda Sakarya illeri arasında konumlanmaktadır. Sapanca Gölü, Kuzey Anadolu Fay Zonu'nun batısında fayın kuzey kolu üzerinde yeralan ve etrafını saran tektonik etkilerle oluşmuş olan bir tatlısu havzasıdır. Göl etrafındaki kompleks tektonik davranış gölün sınırlarını belirleyen ve faylanma sonucunda oluşmuş dağlar ve tepeler ile göl çevresi morfolojisine de yansımıştır.

Türkiye'nin tektonik rejimi üç temel yapı tarafından kontrol edilmektedir. Bunlar Ege-Kıbrıs yayı, sağ-yanal atımlı Kuzey Anadolu Fay Zonu ve sol-yanal atımlı Doğu Anadolu Fay Zonu'dur. Ege-Kıbrıs yayı, güneydeki Afrika plakasının kuzeydeki Anadolu plakasına doğru hareket ederek altına daldığı bir dalma-batma zon sınırıdır. Ayrıca, Arap ve Avrasya plakalarının çarpışması, Anadolu plakasının sağ-yanal atımlı Kuzey Anadolu Fay Zonu ve sol-yanal atımlı Doğu Anadolu Fay zonu boyunca batıya doğru kaçmasına sebep olur.

Kuzey Anadolu Fay Zonu yaklaşık 1600 km'lik uzanımı ve yanal-atımlı fay karakteri ile Türkiye'nin kuzeyindeki tektonik ve morfolojik özellikleri kontrol eden en önemli yapıdır. Kuzey Anadolu Fay Zonu (KAFZ) Marmara Bölgesi'nin kuzeydoğusunda, Sapanca Gölü'nün de üzerinde yeraldığı kuzey ve güney olmak üzere iki ana kola ayrılır. KAFZ dünyanın en aktif fay zonlarından biridir ve yanal yerdeğiştirmeli büyük ölçekli depremler oluşturma potansiyeli yüksektir. 17 Ağustos 1999 İzmit depremi sonucunda fay zonunun kuzey kolunda Sapanca Gölü'nden de geçen yüzey kırıkları oluşmuştur. Bunlar, Sapanca Gölü'nün batısı ve İzmit Körfezi arasında yeralan İzmit-Sapanca Gölü (Sapanca) ve Sapanca Gölü'nün güneydoğu köşesi ve Akyazı (Adapazarı) arasında yeralan Sapanca-Akyazı (Sakarya) segmanlarıdır. Ayrıca, 22 Temmuz 1967 Mudurnu Vadisi depreminin oluşturduğu yüzey kırığı Sapanca Gölü'nün güneyinde yeralır ve doğuya doğru uzanır.

Yüzey kırıkları, depremlerin ve deprem oluşturan fayların anlaşılması açısından doğal bir laboratuvar ortamı oluşturarak Kuzey Anadolu Fayının Sapanca Gölü ve civarındaki konumu ve geometrisi hakkında önemli bilgiler sağlamaktadır. Fakat karadaki bu yüzey kırıklarının Sapanca Gölü içerisine nasıl devam ettiği ve göl içerisindeki fay geometrisi hakkında bu derece kesin yargılara ulaşılamamıştır.

Sapanca Gölü içerisindeki fay yapılanmasını ve geometrisini araştıran araştırmacılar, Sapanca Gölü'nün bir çek-ayır havzası olarak oluştuğu ve Kuzey Anadolu Fayının da göl içerisinde çek-ayır ve sıçrama geometrisi karakterine sahip olduğu konusunda hemfikirdir.

Sığ sismik yansıma yöntemi (Sub-bottom profiling-SBP), sığ ve yüksek frekans içerikli bir çeşit sismik yansıma yöntemidir. Geleneksel sismik yansıma yönteminde olduğu gibi bu yöntemde de akustik ses dalgasının oluşturulma ve kaydedilme prensibi aynıdır; seçilen kaynak su kolonu içerisinde yol alacak ve yer içerisine nüfuz edecek şekilde bir ses dalgası yaratarak deniz tabanı ve yer içerisindeki değişik akustik empedans değerlerine sahip olan tabaka sınırlarından geri yansıyarak alıcı ya da alıcılar tarafından kaydedilir. Bu işlemin birçok defa tekrarlanması sonucunda her bir atışa karşılık gelen izlerin düşey eksen zaman olmak üzere bir araya getirilmesi sonucunda tek ya da çok kanallı profiller (kesitler) elde edilir. Günümüzde kullanılan, değişik frekans, ayrımlılık ve nüfuz derinliği sağlayan çeşitli SBP sistemleri mevcuttur. Yüksek çözünürlük ve yüksek nüfuz derinliği sağlayan yüksek frekanslı 'boomer' en yaygın kullanılan SBP yöntemlerinden biridir. Elektromanyetik prensibe dayalı olarak çalışan 'boomer' ses dalgası kaynağı hem derin hem de sığ sularda deniz sismiği yöntemlerinde sismik kaynak olarak kullanılabilmektedir. Boomer, düz spiral bir bobin tarafından verilen yüksek akımın ön kısımda yeralan alüminyum plakada güçlü eddy akımları meydana getirmesiyle ön plakanın çok yüksek bir hızla itilmesi sonucu oluşan ani ivmenin yarattığı şok dalgasının ses dalgası oluşturması presibi ile çalışır. Kaynağın enerjisi genellikle 100 ile 1000 Joule arasında, frekans bandı ise 300 Hz ile 20 kHz arasında değişmektedir ve yaklaşık 150 m derinliğe kadar nüfuz etmektedir. Gemide bulunan kayıt sistemine bağlı olan boomer kaynağı genellikle bir katamarana monte edilir ve veri toplama sırasında bir tekne ya da gemi tarafından çekilir. Aynı zamanda yine gemi tarafından çekilen ve gemideki kayıt sistemine bağlı olan hidrofon ya da hidrofon dizileri (streamer) ile de sismik kayıt alınır.

Bu çalışma kapsamında, Sapanca Gölü içerisinde konumlandırılan 13 adet hat üzerinde sığ sismik yansıma verileri toplanmıştır. Kaynak olarak sığ sular için de uygun olan yüksek çözünürlüklü 'boomer' kullanılmıştır. Hatların uzunlukları ve konumları coğrafi, çevresel ve operasyonel koşullarla sınırlanmış olsa da yine TÜBİTAK-1001 117Y130 no'lu proje kapsamında, sismik yansıma çalışmasından önceki aşamalarda toplanan çok-ışınlı batimetri verisindeki değişimler göz önünde bulundurularak belirlenmiştir.

Boomer sismik yansıma verilerinin veri işlemi, İstanbul Teknik Üniversitesi Jeofizik Mühendisliği Bölümü Nezihi Canıtez Veri İşlem Laboratuvarı'nda gerçekleştirilmiştir. Veri işlem, çeşitli matematiksel işlemler ile verinin birtakım özelliklerinin değiştirilerek yer içerisine ait daha net bir görüntü elde etme işlemi olarak tanımlanabilir. Bu nedenle, verinin doğru şekilde işlenmesi ve temel karakteristik özelliklerini kaybetmemesi veri işlem sonrasındaki yorumlama aşamasında elde edilen sonuçların güvenilirliği açısından kritik rol oynamaktadır. Çalışma alanının küçük olması ve toplanan tüm hatlara ait verilerin benzer özellikler göstermesi nedeniyle veri işlem aşamasında gerçekleştirilen testler sonuncunda elde edilen en uygun veri işlem parametreleri tüm hatlara aynı şekilde uygulanmıştır. Veri işlem aşamaları sırasıyla, filtreleme, dekonvolüsyon, ikincil (dekonvolüsyon sonrası) filtreleme, iz dengeleme (trace balancing) ve migrasyon işlemleridir. Bunların yanısıra her bir hatta filtreleme öncesi ve migrasyon sonrası su-tabanı silme (mute) işlemi uygulanmıştır. Sismik veriler hem sinyal hem de gürültü içerirler. Sinyal yer içinin doğru biçimde yorumlanması için kullanılan, gürültü ise sinyali maskeleyen,

dolayısıyla atılmak istenen kısımdır. Filtreleme işlemi bu istenmeyen gürültülerin veriden atılmasını sağlayan veri işlem aşamasıdır. Bir sismik iz ya da sismogram yer içinin kaynak dalgacığına ve kayıt sistemine verdiği yanıttır. Bu nedenle, sismik iz, bir dizi yansıma katsayısından oluşan yansıma fonksiyonu ve gürültü ile kaynak dalgacığının konvolüsyonunun ürünü olarak tanımlanabilir. Dekonvolüsyon ise gürültülerin ayıklandığı ve kaynak dalgacığının etkilerinin ortadan kaldırılarak sadece yansıma fonksiyonun elde edildiği ters konvolüsyon işlemi olarak tanımlanabilir. İz dengeleme genellikle dekonvolüsyon işleminden sonra uygulanan, zamandan bağımsız bir ölçekleme yöntemidir. Denge faktörü, belirlenen pencere aralığında hesaplanan RMS genliklerinin arzu edilen RMS genliklerine oranı olarak tanımlanır. Sismik dalgaların yer içerisinde yüzeyin direkt olarak altındaki bir noktadan yansıdığı durumlar ancak yer içerisindeki tabakaların tam olarak yatay olması şartıyla gerçekleşebilir. Fakat yer içinin karmaşık yapısı düşünüldüğünde bu nadiren mümkün olur. Sismik migrasyon işlemi sismik kesiti yeniden yapılandırarak yansımaları gerçek konumlarına taşıma işlemidir.

Veri işlem aşamasından sonra elde edilen tüm migrasyon kesitleri yorumlanarak Sapanca Gölü'ne ait bir fay haritası oluşturulmuştur. Yorumlar, maksimum kayıt uzunluğu olan 150 ms'lik kesitler üzerinde yapılmıştır. Fakat kesin yorumlar, kesitlerin tekrarlı yansımalarla maskelenmiş olması ve de kullanılan sismik kaynağın yüksek frekans içeriğinden dolayı nüfuz derinliğinin kısıtlı olması nedeniyle, ilk 50-100 ms arasında sınırlı kalmıştır. Kesitlerini yorumlanması sonucunda, Kuzey Anadolu Fayı hemen hemen tüm hatlarda göl tabanında küçük çaplı kıvrımlar oluşturan ve derinlere inildikçe her iki tarafında yer alan sedimanları etkileyen düşey bir süreksizlik olarak gözlenmiştir. Sismik kesitlerde gözlenen bu süreksizlikler çok-ışınlı batimetri verilerinde gözlenen çizgiselliklerle ilişkilendirilebilmektedir. Migrasyon kesitlerinin çok-ışınlı batimetri verisi ile karşılaştırılarak yorumlanması sonucunda oluşturulan fay haritası incelendiğinde, güneydoğu ucundan göle giren ve yaklaşık 5 km boyunca B-KB uzanımlı olarak harita düzlemi ile 30°'lik bir açı yaparak ilerleyen ve daha sonra hafif yön değiştirerek batıya doğru 5 km daha devam ettikten sonra kuzeybatı uçtan gölü terkeden Kuzey Anadolu Fayı, Sapanca Gölü boyunca takip edilebilmektedir. Kuzey Anadolu Fayı'nın bu geometrisi gevşeyen büklüm (releasing bend) fay karakteri ile örtüşmektedir. Ayrıca, gölün güney kısmında tanımlanan ve yanal-atımlı fay karakteri gösteren bir diğer faylanma yapısının 22 Temmuz Mudurnu Vadisi Depremi sonucu oluşan yüzey kırığı ile ilişkili olduğu düşünülmektedir. Gölün güneybatısında tanımlanan bir başka yanal-atımlı olduğu düşünülen fay ile ilgili sismik hatta komşu kesitlerde aynı yapıya rastlanamamış olması ve bu bölgede savı destekleyecek çok-ışınlı batimetri verisinin de olmaması nedeniyle bu faylanmayla ilgili net bir sonuca varılamamıştır. Son olarak, gölün batı kısmındaki hatlarda gözlenen küçük ölçekli fay grupları gaz sızıntıları ile ilişkilendirilmiştir.

1. INTRODUCTION

The North Anatolian Fault Zone (NAFZ) is one of the most seismically active fault zones in the world which produces large magnitude earthquakes with mostly strike-slip displacements. NAFZ is an intracontinental right-lateral strike-slip transform fault (Ketin, 1948 as cited in Alpar and Yaltırak, 2002) extending across northern Turkey and defining the boundary between the Anatolian and Eurasian plates (Ketin, 1969; Şengör et al., 1985; Barka,1992; Şaroğlu, 1988 as cited in Alpar and Yaltırak, 2002).

In the eastern Marmara Region, the NAFZ splits into two strands and the study area, Lake Sapanca, is located in the northern strand between Gulf of İzmit in the west and Adapazarı in the east where had been identified as a 150-km-long seismic gap by Toksöz et al. (1979) prior to the two large 1999 İzmit and Düzce earthquakes. NAFZ is shown in Figure 1.1 along with the earthquake focal mechanism from 1939 to 2012 superimposed along the fault zone. The 17 August 1999 İzmit and 12 November 1999 Düzce earthquakes were the last two largest events occurred on the NAFZ between which the study area, Lake Sapanca, lays (Figure 1.2).

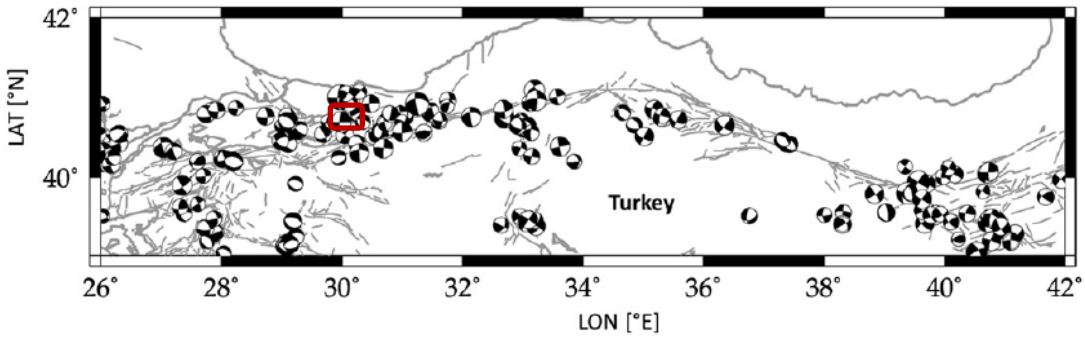

Figure 1.1 : The North Anatolian Fault Zone (NAFZ) and earthquake focal mechanisms the years 1939–2012 (Bohnhoff et al., 2016). Red box indicates the location of the study area, Lake Sapanca.

During 17 August 1999 İzmit earthquake, two segments, Sapanca (İzmit- Lake Sapanca) segment in the west and Sakarya (Sapanca-Akyazı) segment in the east of the lake were ruptured which were investigated and mapped by numerous researchers such as Barka et al. (2002) and Lettis et al. (2002) (Figure 1.2).

As well as providing a natural laboratory environment for the study of the earthquakes and earthquake-producing faults, surface ruptures are clear representations of the location and the extension of the NAFZ around Lake Sapanca. However, little was known regarding how these ruptures extended through offshore Lake Sapanca until the detailed study of Lettis et al. (2002) based mainly on bathymetric data of the lake (Figure 1.3); of Gürbüz and Gürer (2008b) based on the morphology and geologic setting of the lake and its vicinity; and of Gülen et al. (2014) based on the bathymetry and seismic reflection data acquired in the lake.

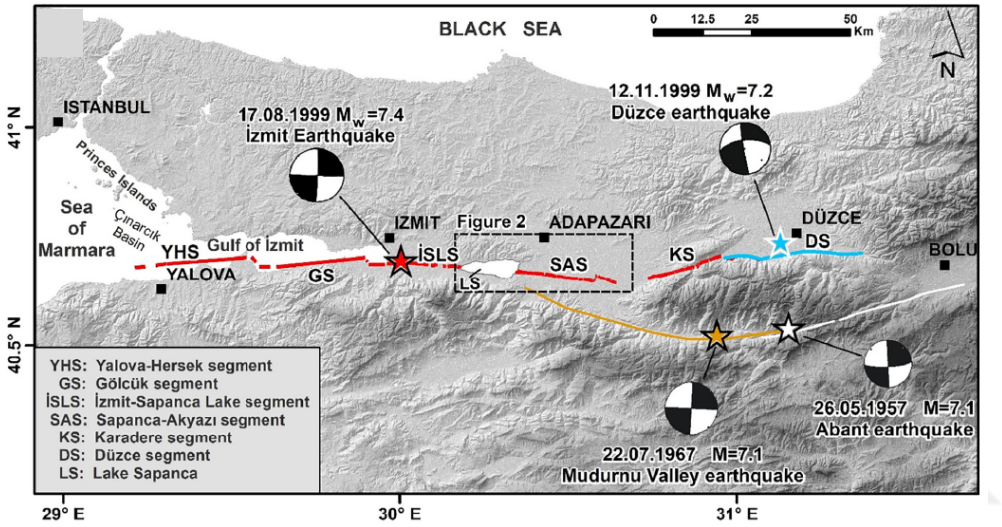

Figure 1.2 : Surface ruptures (colored lines) of large earthquakes with epicenters (stars) and relevant focal mechanisms around Lake Sapanca in the eastern Marmara region (Dikbaş et al., 2009).

All three studies support each other's findings, which are presented in detail in the following chapter, and meet at the common conclusion that Lake Sapanca has a pull-apart fault geometry.

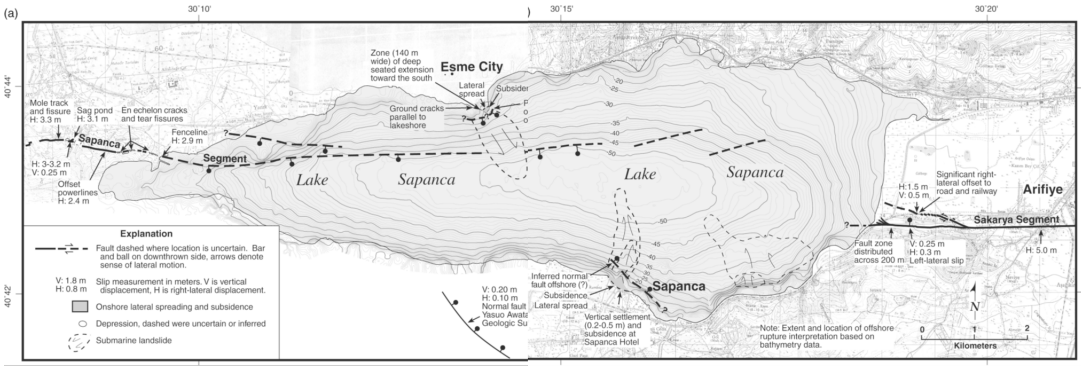

Figure 1.3 : Detailed hypothetical submarine tectonics of Lake Sapanca and surrounding fault segments on land derived from the surface ruptures of 17 August 1999 İzmit earthquake (modified with images merged from Lettis et al., 2002).

This study is carried out using the thirteen sub-bottom profiling lines (shallow seismic reflection profiles) and the bathymetry measurements acquired in the scope of TÜBİTAK-1001 project (Project No: 117Y130). The aim of the study is the application of common marine seismic data processing techniques on a Boomer-sourced, high-resolution shallow marine seismic reflection (Boomer sub-bottom profiling) data collected in Lake Sapanca, Turkey, the interpretation of the processed sections, and furthermore, to determine the characteristics of the active submarine tectonism in Lake Sapanca.

2. STUDY AREA

The study area, Lake Sapanca, is situated in the northwest Turkey between Izmit in the west and Sakarya in the east in the eastern Marmara region (Figure 2.1). Lake's longest distances from west to east and north to south are approximately 15.8 km and 5.5 km, respectively, with an approximate surface area of 47 km^2.

Figure 2.1 : Location of Lake Sapanca, Turkey (retrieved from Google Earth).

Lake Sapanca is a freshwater basin created by faulting and is located in the western strand of the North Anatolian Fault Zone (NAFZ) and lies on a tectonically complex area which is well-reflected by the neighboring morphology consisting of a series of

fault-generated mountain ranges defining the boundaries of the lake (Gürbüz and Gürer, 2008a and Gürbüz and Gürer, 2008b).

2.1 Geology of Lake Sapanca and the Vicinity

Lake Sapanca is situated on the northern strand of the North Anatolian Fault Zone (NAFZ) on the İzmit-Sapanca Corridor and it is bordered by a series of mountain ranges. These mountain ranges are composed of Paleozoic to Early Tertiary metamorphic and sedimentary rocks which form the basement of the region (Gürbüz and Gürer, 2008a). Figure 2.2 shows the geological settings in Lake Sapanca area.

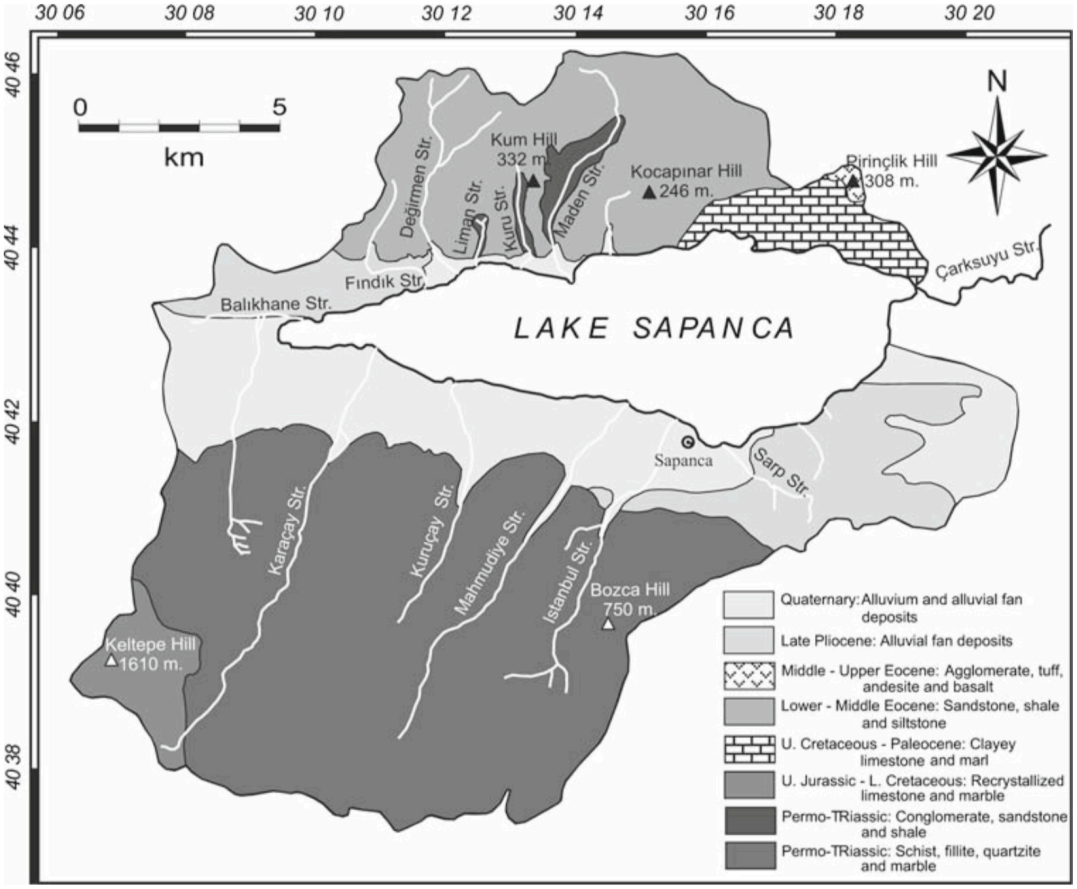

Figure 2.2 : Geological and hydrological map of Lake Sapanca and nearby area (Gürbüz and Gürer, 2008a).

Samanlı mountains in the south which were raised as a pressure ridge structure and isolated from the nearby morphology between the northern and southern elements of the NAFZ (Koçyiğit, 1988 as cited in Gürbüz and Gürer, 2008b) consist of Paleozoic-Mesozoic rocks which include metamorphic rocks schist, marble, gneiss and quartzite and meta-ophiolitic rocks peridotite, gabbro and amphibolite in the Sapanca front of

the mountains which is situated in the southern limit of Lake Sapanca (Gürbüz and Gürer, 2008a).

Paleozoic-Early Tertiary rocks consisting of sandstone, clayey limestone, marl and interbedded sandstone, shale and siltstone crop out as uplifted basement against the Plio-Quaternary units on the Eşme front of the Kocaeli Peneplane (Figure 2.2) (Gürbüz and Gürer, 2008a).

Lake Sapanca's sea floor is filled with Plio-Quaternary alluvial fan and alluvium deposits (Gürbüz and Gürer, 2008a).

2.1.1 Formation of Lake Sapanca

A lake is an area filled with water surrounded by land and localized in a basin which are bowl-shaped depressions in the Earth's surface. Lakes are different from lagoons since they are not part of the ocean and lie on land. Lakes are also bigger and deeper than ponds, most of which are nourished and depleted by rivers and streams.

Natural lakes are usually originate in rift zones, mountainous areas and in areas where glaciation process is ongoing while others can be found in endorheic basins, which is a closed drainage basin with no water flow to other external bodies of water, such as rivers or the ocean, or along the paths of mature rivers.

Based on the process of forming, natural lakes can be classified as volcanic, tectonic, glacial, fluvial, solution, landslide, aeolian, shoreline, organic and meteorite (crater) lakes. Surrounded by active faults and mountains, Lake Sapanca most likely falls into the category of tectonic lakes as the opinions regarding its formation suggest as some of which are given below. Tectonic lakes are created by lateral and vertical movements which include faulting, tilting, folding, pulling and twisting in the Earth's crust resulting in deformation and distortion.

Lettis et al. (2002) interpreted a bathymetric data of Lake Sapanca and concluded that a fault segment outlines the northern edge of the lake basin and lengthens across Lake Sapanca to the eastern edge of the lake forming the lake basin by a right step-over or parting between the fault segments.

According to Gürbüz and Gürer (2008b), surface rupture of 17 August 1999 earthquake cutting across the İzmit-Sapanca Corridor developed as a cross-basin fault in an asymmetrical pull-apart basin indicating that this basin is in the mature stages of

evolution. Therefore, the authors suggested that Lake Sapanca formed as a pull-apart basin created by the cross-basin fault in this asymmetrical pull-apart basin.

For their study, Gülen et al. (2014), produced a detailed bathymetry map of Lake Sapanca and in combination with interpretation of the seismic reflection data collected in the lake, they concluded upon the existence of a pull-apart fault geometry in Lake Sapanca which coincides with Gürbüz and Gürer (2008b)'s findings. The authors also speculated that Lake Sapanca is a basin formed by depression controlled by the surrounding structural elements.

Furthermore, Gürbüz et al. (2010) studied the connection of the Sea of Marmara, Lake Sapanca and Black Sea through an alternative strait to the north of Lake Sapanca. The researches based their studies on the historical documents over the last 2500 years indicating an impermanent presence of water in parts of the İzmit-Sapanca Corridor. They suggested that the existence of small sills higher than the lake level in a couple of locations between Lake Sapanca and İzmit Gulf might support the idea, however, there is no known signs of fluviatile or marine sediments, therefore, a proof of existence of an ancient connection is inconclusive.

2.2 Active Tectonics of Turkey and the Study Area

Tectonic regime in Turkey is ruled by three main elements; the Aegean-Cyprean Arc, the dextral North Anatolian Fault Zone and the sinistral East Anatolian Fault Zone which are shown in Figure 2.3 (Bozkurt, 2001).

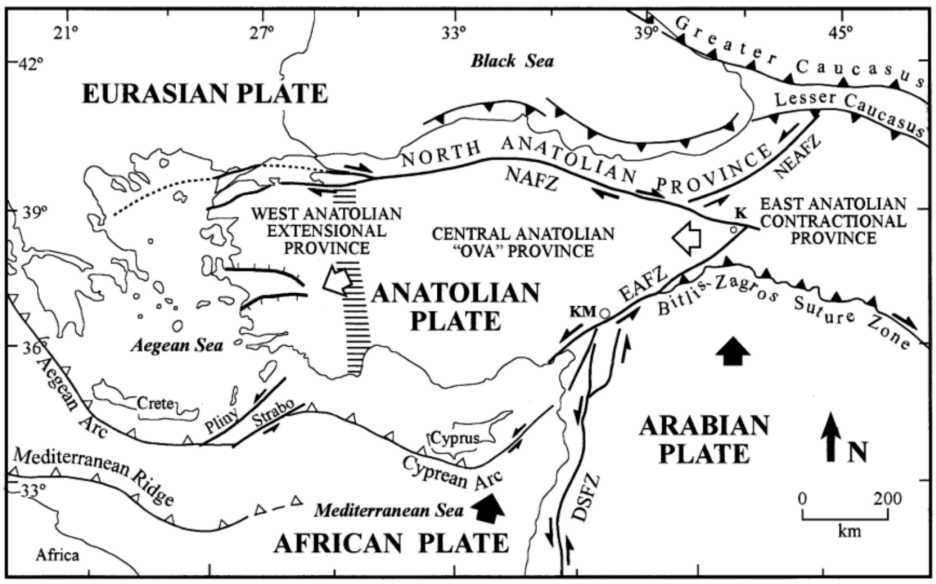

Figure 2.3 : Simplified tectonic map of Turkey and surroundings (Bozkurt, 2001).

The Aegean-Cyprean Arc is a convergent plate boundary where the African Plate to the south is subducting beneath the Anatolian Plate to the north. The dextral North Anatolian Fault Zone and the sinistral East Anatolian Fault Zone are intracontinental strike-slip faults along which the Anatolian Plate moves westward away from the collision zone between the Arabian and the Eurasian plates (Şengör et al., 1981 and 1985 as cited in Bozkurt, 2001). The two strike-slip faults encounter and create a continental triple junction to the east of Karlıova in the north-eastern Turkey and the Anatolian Plate which is extruded in the westward direction also carries an anticlockwise rotation which is associated with a tectonic escape (McKenzie, 1970; Dewey and Şengör, 1979; Rotstein, 1984; Jackson and McKenzie, 1988; Westaway, 1994; Oral et al., 1995 and Seber et al., 1997 as cited in Bozkurt, 2001).

2.2.1 North Anatolian Fault Zone (NAFZ)

The NAFZ, which was first described by Ketin (1948), with its 1600 m length and dextral strike-slip characteristic, is the most important element that governs the recent tectonic and morphologic development of the northern part of Turkey. It extends from the Karlıova triple junction in the east Anatolia toward the İstanbul–Marmara region following a northern trending path (Figure 2.4).

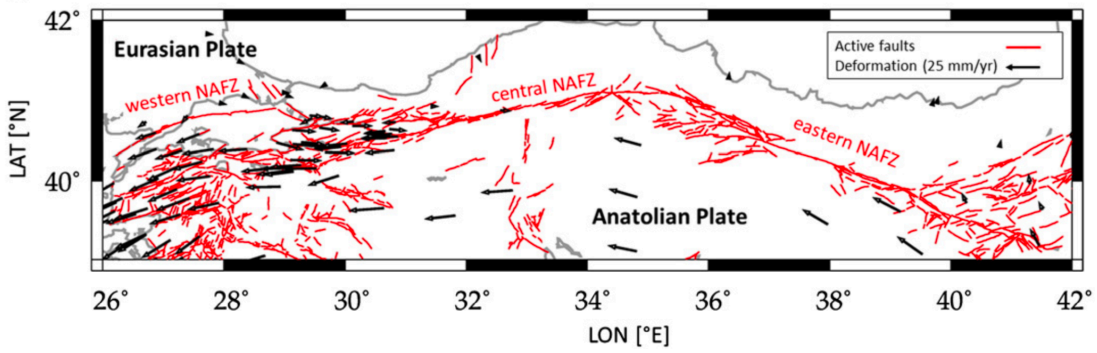

Figure 2.4 : Tectonic setting of the NAFZ in Turkey showing fault segments (red lines) (Turkey General Directorate of Mineral Research and Exploration) and GPS-derived horizontal velocity field of the Anatolian plate with respect to static Eurasia (black arrows) (after McClusky et al., 2000) (Bohnhoff et al., 2016).

The NAFZ formed in relation to the northward moving Arabian Plate in the east and the southward rollback of the Hellenic subduction zone in the west (Armijo et al., 1999; Flerit et al., 2004; LePichon et al., 2015 as cited in Bohnhoff et al., 2016). The current slip rates are approximately 20 mm/year in the east and 25 mm/year in the west

(Barka, 1992; McClusky et al., 2000 and Reilinger et al., 2006 as cited in Bohnhoff et al., 2016).

The NAFZ's main faulting mechanism is right-lateral strike-slip, however, in the western part, earthquakes with normal faulting has been observed as a result of the transtensional structure produced by the slab pull of the Hellenic subduction zone (Flerit et al., 2004 and Bohnhoff et al., 2005 as cited in Bohnhoff et al., 2016). Transpression was not seen along the whole fault zone as the earthquake source mechanisms suggested (Şengör et al., 2005 and Ekström et al., 2012 as cited in Bohnhoff et al., 2016).

The fault splits into two major branches; the northern branch on which Lake Sapanca is located and the southern branch in the north-east of Marmara Region. According to the GPS measurements, the northern strand is more active with approximate slip rate of 10-15 mm/year (Straub et al., 1997 as cited in Lettis et al., 2002) (Figure 2.5).

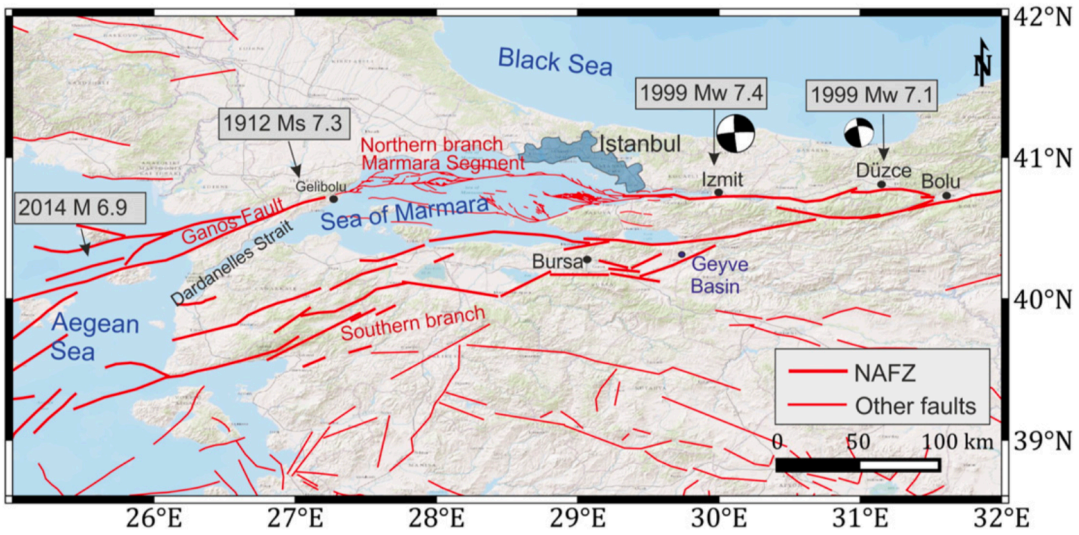

Figure 2.5 : Map of the western part of the NAFZ. Major recent earthquakes are indicated by year and magnitude pointing to the epicenter. Focal mechanisms of the 1999 İzmit and Düzce earthquakes are also shown (Bohnhoff et al., 2016).

The northern strand of NAFZ contains the segments which slipped during the 17 August 1999 Kocaeli earthquake of which the surface rupture passes through Lake Sapanca (Figure 2.6) (Barka et al., 2002 and Lettis et al., 2002).

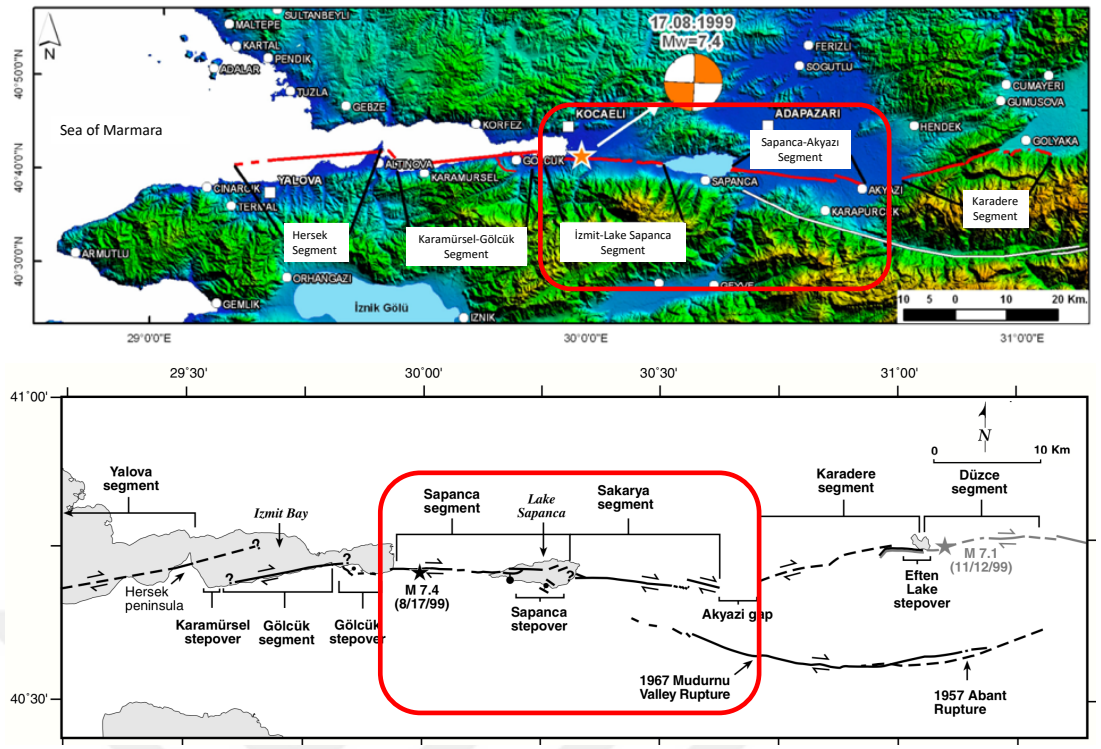

Figure 2.6 : Location of the fault ruptures on either side of Lake Sapanca associated with the 17 August 1999 earthquake from Barka et al. (2002) (top) and from Lettis et al. (2002) (bottom).

2.2.1.1 İzmit-Lake Sapanca segment

İzmit-Lake Sapanca segment extends between Gulf of İzmit and the west of Lake Sapanca in the east-west direction. The total length of the segment is around 25 km, 19 km of which is on land (Figure 2.7) (Dikbaş, 2009).

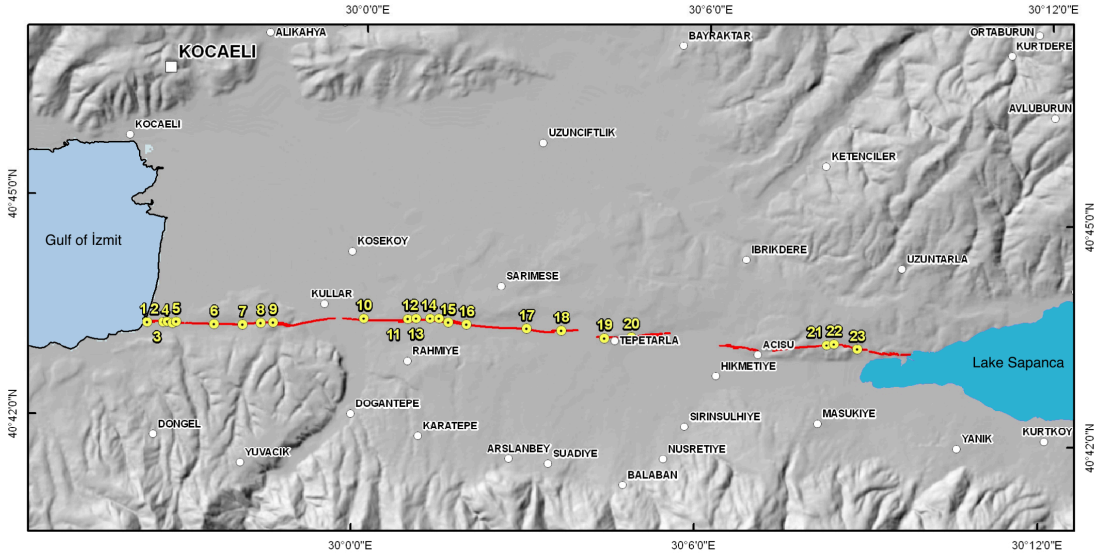

Figure 2.7 : Surface rupture of 1999 İzmit earthquake on İzmit-Lake Sapanca segment and the locations of the displacement measurements (Dikbaş, 2009).

The segment enters Lake Sapanca from the northwest of the lake forming step-overs along the way in the west and the east of Tepetarla. The maximum right-lateral displacement measured on the segment is approximately 3 m where the average displacement is 2.1 m.

2.2.1.2 Sapanca-Akyazı segment

Sapanca-Akyazı segment extends from the south-east corner of Lake Sapanca to the further east as it makes a left step-over in the west of Akyazı (Adapazarı) and terminated in the north of the town (Figure 2.8) (Langridge et al., 2002 as cited in Dikbaş, 2009).

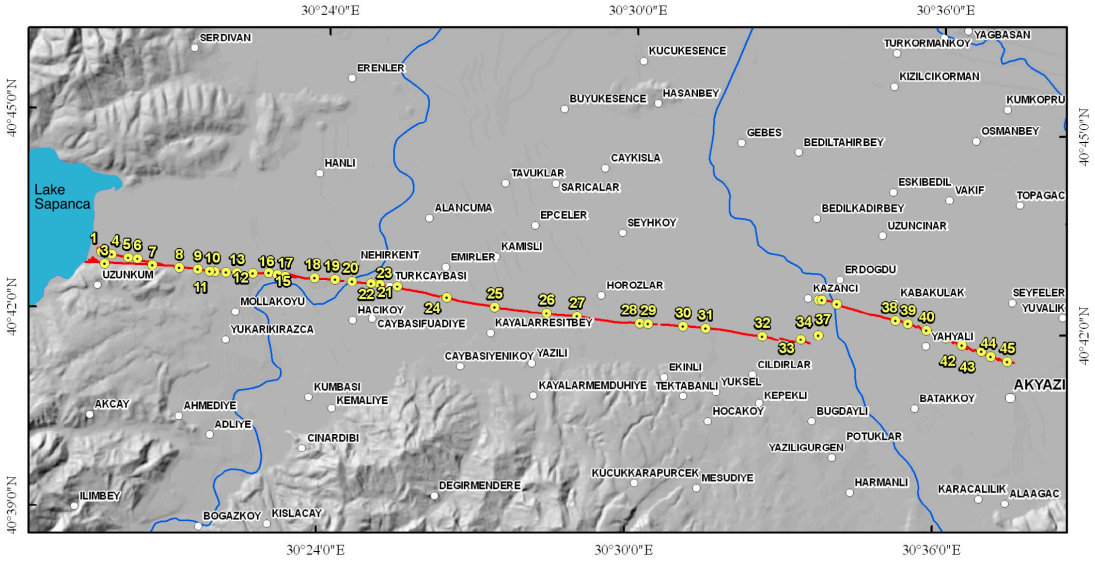

Figure 2.8 : Surface rupture of 1999 İzmit earthquake on Sapanca-Akyazı segment and the displacement measurements (Dikbaş, 2009).

The total length of the segment is around 25 km and the longest displacement value measured on the segment, 5.1 m, was in the town of Arifiye which was the largest displacement occurred as a result of the 17 August 1999 İzmit earthquake (Barka et al., 2002 and Langridge et al., 2002 as cited in Dikbaş, 2009).

2.2.1.3 Mudurnu fault

Mudurnu fault which ruptured during the 1967 Mudurnu Valley earthquake is located in the south of Lake Sapanca and extends towards the east (Figure 2.9) (Ambraseys and Zatopek, 1969).

Ambraseys and Zapotek (1969 as cited in Dikbaş, 2009) mapped the surface rupture of the Mudurnu Valley earthquake starting from Lake Abant in the east to the south of

Karapürçek (Adapazarı) in the west. After this 50-km-long section, the surface rupture was indicated with dashed line towards the south of Lake Sapanca which increases the total length of the rupture to approximately 80 km. The authors stated that the eastern 25 km of the surface rupture collided with the rupture of the 26 May 1957 Abant earthquake and even passed through the same locations in some places.

Figure 2.9 : Surface rupture of 22 July 1967 Mudurnu Valley earthquake (digitized from Ambraseys and Zapotek 1969) (Dikbaş, 2009).

The length of the deformation on which the surface rupture is identified is 1-3 km and the maximum right-lateral displacement caused by the faulting is 1.9 m where the vertical displacement is 1.2 m (Ambraseys and Zapotek, 1969 as cited in Dikbaş, 2009).

2.2.1.4 Submarine tectonics of Lake Sapanca

Although there is physical evidence with regards to the fault structures surrounding Lake Sapanca as stated in the previous subsections, what has been happening beneath the lake in terms of tectonic characteristics has only been studied over the last two decades.

In their study, Lettis et al., (2002) described each step-over basin associated with 1999 İzmit earthquake, and with the aid of bathymetry data they collected in Lake Sapanca right after the earthquake, the authors defined the characteristics, dimensions and fault geometry within offshore Lake Sapanca (Figure 2.10). The authors determined that the Sapanca basin formed at right-parting step-over between the Sapanca (İzmit-Lake Sapanca) and Sakarya (Sapanca-Akyazı) segments and the right-releasing twist and step-over to the Mudurnu branch of the NAF.

Bathymetry data indicated that basin is margined with the Sapanca fault segment in the north and with spread out normal faulting in the south. The Sakarya segment does not seem to continue offshore into the Lake Sapanca along the southern border of the basin where the Sapanca fault segment expands across almost the entirety of the lake to the eastern boundary.

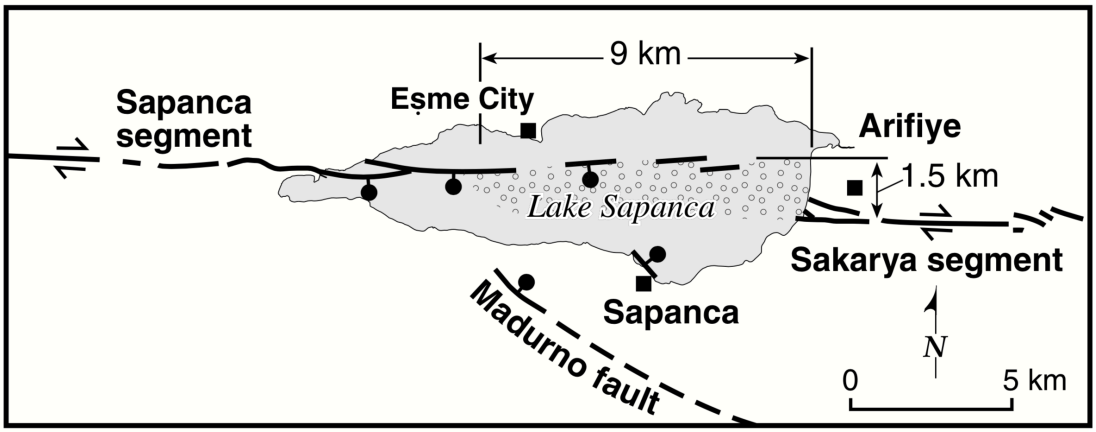

Figure 2.10 : Fault segments in western and eastern margins of Lake Sapanca and speculated fault locations in the lake (Lake Sapanca step-over) (Lettis et al., 2002).

A sequence of northwest-trending normal faults dominates the southern boundary of Lake Sapanca along with the Mudurnu Valley segment of the southern strand of the NAF meeting the Sapanca segment at the lake.

Using geomorphic and morphometric information in combination with the bathymetric data, Gürbüz and Gürer (2008a), studied the spatial differences of the Plio-Quaternary tectonic activity and deformation of different fault segments of the NAFZ in the eastern Marmara region and Lake Sapanca which are represented in Figure 2.11.

The authors stated that the fault geometry is defined by the mountain-front faults on both northern and southern margins of Lake Sapanca in the İzmit-Sapanca Corridor and based on the geomorphic and morphometric investigations, it was determined that the southern mountain-front fault which displayed characteristics of a master fault is more active than the northern fault which was proposed as antithetic fault of this master fault. Finally, it was concluded that the surface rupture created by 17 August 1999 earthquake cutting across the İzmit-Sapanca Corridor formed as a cross-basin fault in an asymmetrical pull-apart basin which is usually defined by a master fault on one side of the basin and the basin axis close to the master fault (Rahe et al., 1998 as cited in

Gürbüz and Gürer, 2008b), and Lake Sapanca developed as another pull-apart basin in this asymmetrical pull-apart basin.

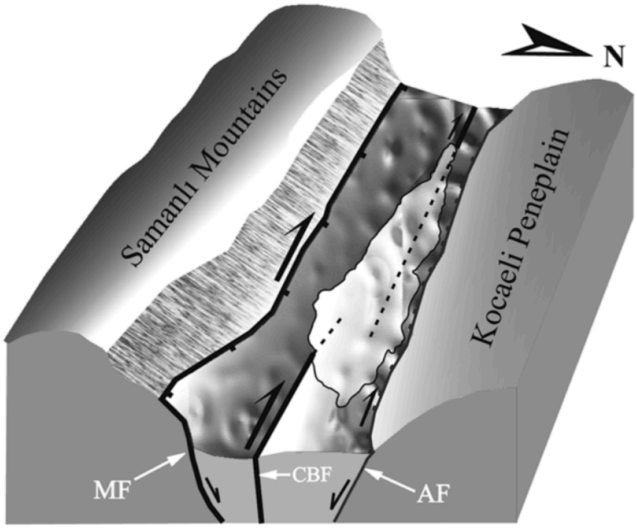

Figure 2.11 : Schematic block diagram showing the different fault segments of the NAFZ that developed as an asymmetric pull-apart basin. MF: Master fault. CBF: Cross-basin fault (1999 earthquake rupture). AF: Antithetic fault (Gürbüz and Gürer, 2008b).

In order to reveal the structural elements responsible for the formation of Lake Sapanca and to create an active fault map of the lake, Gülen et al. (2014), acquired seismic reflection and side-scan sonar data in Lake Sapanca. By interpreting the seismic sections, the researchers mapped the active faults residing in the lake as well as concluding on the existence of a pull-apart fault geometry in the lake as part of the NAFZ and an east-west trending en-échelon fault system (Emre et al., 2003 as cited in Gülen et al., 2014) leaving the lake at the location predicted by Lettis et al. (2002) in the western part of the lake. Gülen et al. (2014)'s active fault map of Lake Sapanca is shown in Figure 2.12.

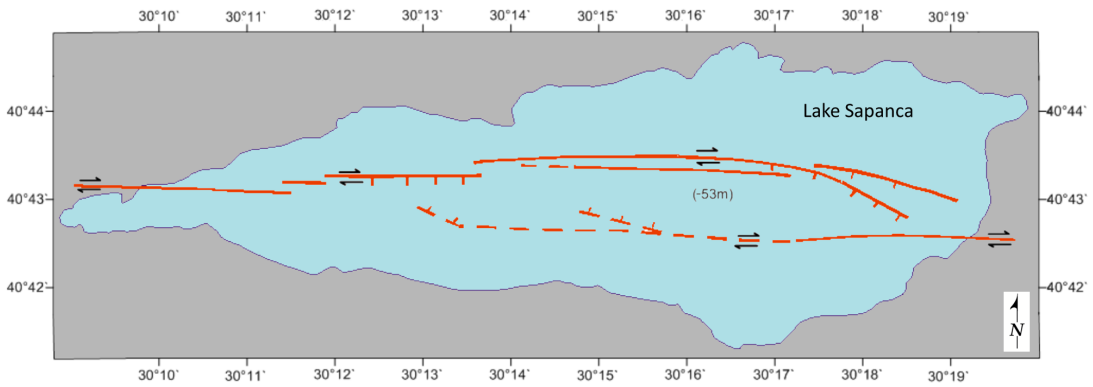

Figure 2.12 : Lake Sapanca active fault map (Gülen et al., 2014).

3. METHOD AND DATA ACQUISITION

3.1 Sub-bottom Profiling

Sub-bottom profiling (SBP) is a type of seismic reflection method which is used for shallow reflection seismic profiling operating at broader range of frequencies. Generation and detection of an acoustic wave is the common basic principle of the seismic reflection methods. Based on the same principle, in sub-bottom profiling, the source generates a short pulse of sound (shot) which travels through the water entering the seabed and the energy is reflected back from the boundaries between subsurface layers of differing acoustic impedance (Stoker et al., 1997). The reflected energy is sensed by a hydrophone or hydrophone array and recorded as a trace which then accumulated and displayed next to each other against time creating a profile (section) (Stoker et al., 1997).

There are several types of sub-bottom profiling systems with various operating frequencies, resolution and penetration depths. Common types of SBP systems and their acoustic characteristics are listed in Table 3.1.

Table 3.1 : Commonly used sub-bottom profiling systems and their properties (modified after Ramsey, Peter. *Sub-bottom Profiling Acquisition Techniques in HYPACK®* 20 Mar, 2019).

System	Operating Frequency	Typical Resolution	Typical Depth of Penetration	Trigger Interval
Chirp	2 – 16 kHz	0.05 – 0.1 m	5 – 50 m	250 ms
Parametric SBP	2 – 22 kHz	0.05 – 0.1 m	5 – 30 m	-
Pinger	2 –12 kHz	0.2 m	10 – 50 m	250 ms
Bubble Pulser	0.4 kHz	0.3 - .0.5 m	20 – 100 m	-
Boomer	0.3 – 6 kHz	0.2 - 0.5 m	20 – 150 m	500 ms
Sparker	0.2 – 3 kHz	0.3 – 1 m	30 – 750 m	500 ms – 1 s
Mini Airgun	0.1 - 3 kHz	0.5 – 1 m	30 – 200 m	1 s – 2 s

The high-frequency “boomer”, which is used for this study, is one the most commonly used sub-bottom profilers providing high resolution and deep subsurface penetration. Elements of a vessel-towed sub-bottom profiler (SBP) system operating with a Boomer source and a single hydrophone are shown in Figure 3.1.

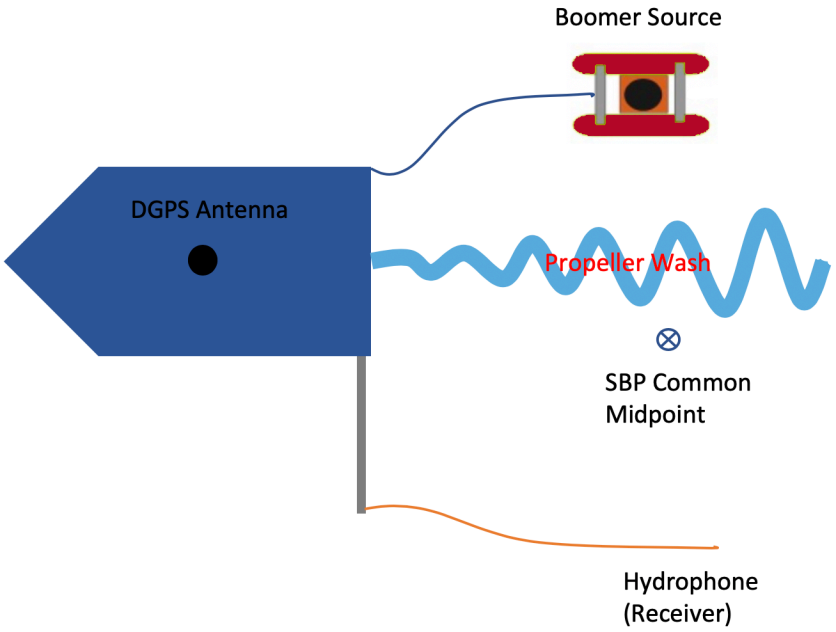

Figure 3.1 : Elements of vessel-towed sub-bottom profiler (SBP) system with Boomer source (modified after Ramsey, Peter. Sub-bottom Profiling Acquisition Techniques in HYPACK® 20 Mar, 2019).

3.2 Boomer Sound Source

The Boomer source is an electromagnetically driven sound source (Edgerton and Hayward, 1964) which has been utilized as a marine seismic source for reflection surveys in deep and shallow water for over five decades and has been considered an easy-to-use, reliable and durable type of seismic source (Simpkin, 2005). Furthermore, with its ultra-high bandwidth signature, by using standard seismic data processing, high resolution and high signal-to-noise ratio, thus high data quality can easily be achieved (Simpkin, 2005).

The boomer consists of a transducer which is the sound-producing component, an electronic power supply, a capacitor and a triggering device (Edgerton and Hayward, 1964). The boomer transducer is a flat coil of wire which is magnetically coupled to either one or two aluminum plates. In Figure 3.2, schematic diagram of a boomer sound source and a typical arrangement of the discharge circuitry are shown.

In the boomer, a heavy flow of current is discharged through a flat spiral coil inducing strong eddy currents in the aluminum front plate. Then the mutual repulsion pushes the front plate outward flexing away from the coils with high acceleration generating sound as this flexing creates an acoustic shock wave (Edgerton and Hayward, 1964).

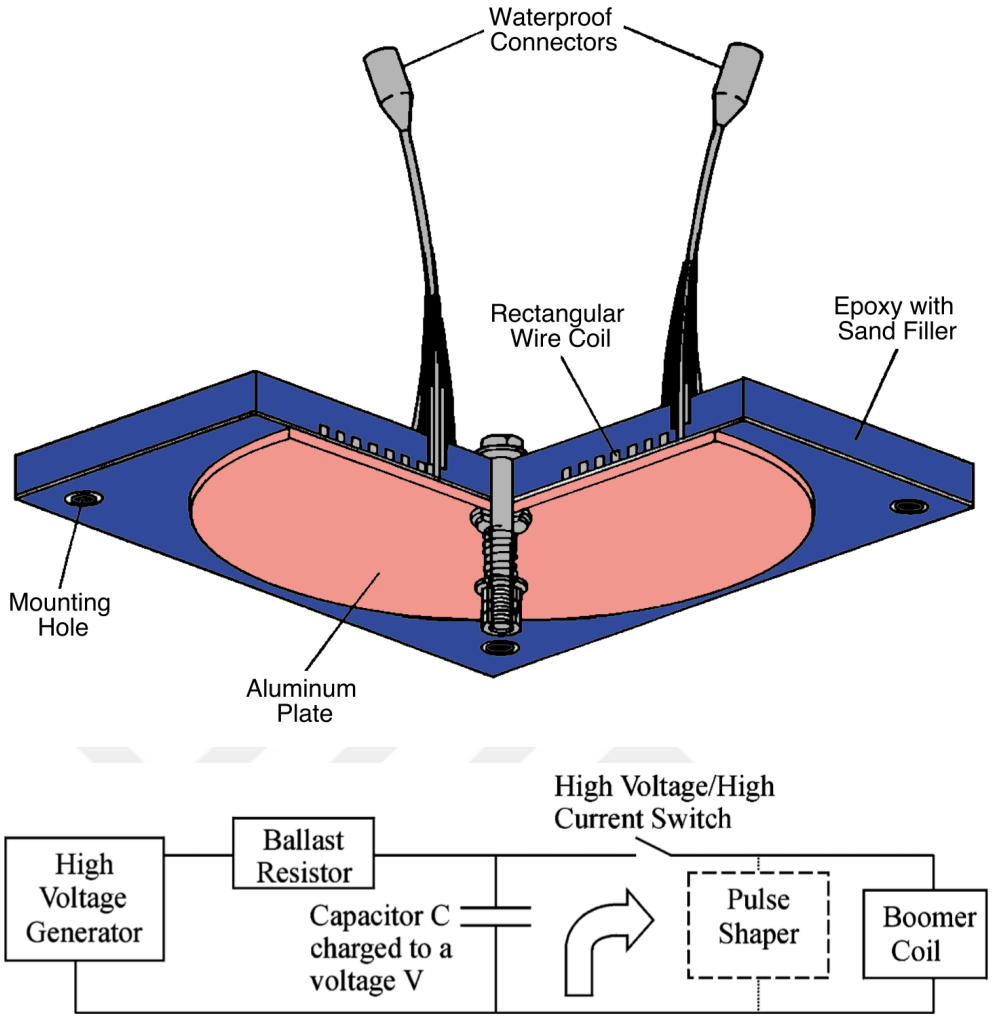

Figure 3.2 : Schematic diagram of a Boomer source on top (modified from Edgerton and Hayward, 1964) and a typical arrangement of the discharge circuitry (Simpkin et al., 2005).

Energy of the source depends on the capacitor bank, which is typically ranging between 100 and 1000 J. Broad spectrum of highly repeatable boomer source signatures can range from 300 Hz–20 kHz and centimeter-precision resolution and up to 150-m penetration can be achieved (Tóth, 2011).

The boomer source is usually mounted on a towed catamaran, which is towed behind a boat along with a separate single hydrophone or hydrophone array (streamer) as a receiver which are connected to a recording system onboard the towing vessel (Figure 3.1).

3.3 Acquisition of Boomer-Sourced Seismic Reflection Data

In this study, thirteen seismic reflection profiles, which are numbered B1-B13 from west to east, were acquired in Lake Sapanca using a single-receiver, Boomer-sourced sub-bottom profiling method which is high-resolution and suitable for shallow waters. Total of 52 km of seismic reflection data was collected as part of the TÜBİTAK-1001 project (Project No: 117Y130) in August 2018. Location of the profiles are shown in Figure 3.3 and start of line (first shot point) and end of line (last shot point) coordinates in UTM are given in Table 3.2.

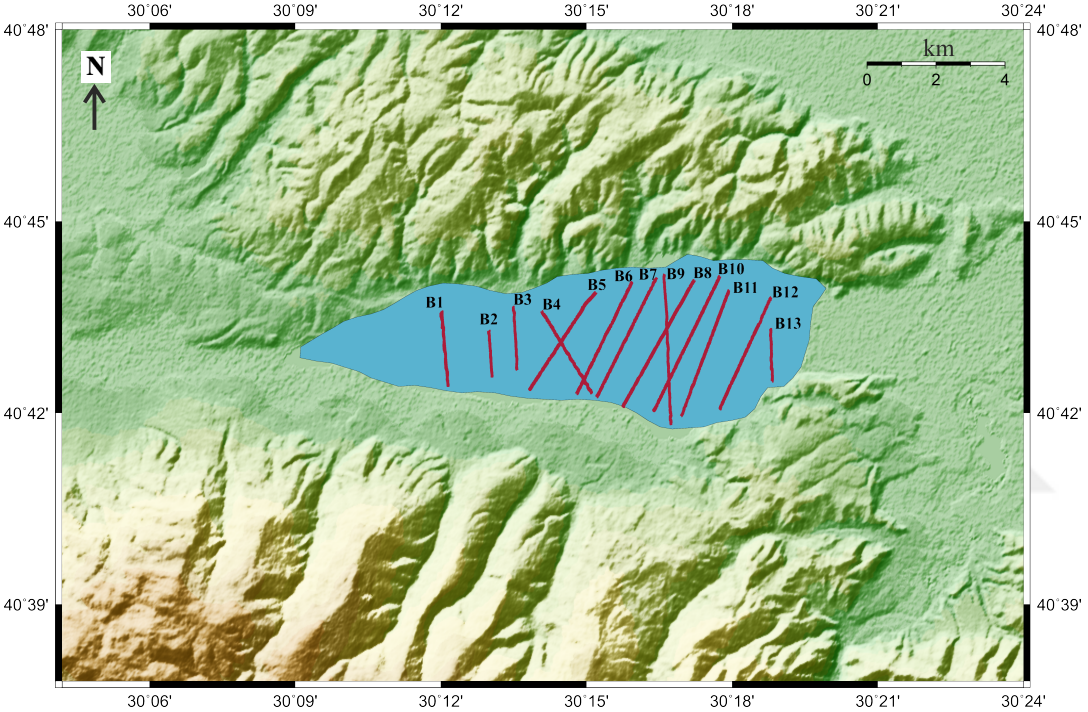

Figure 3.3 : Location of the "Boomer" profiles in Lake Sapanca. Map created using GMT (The Generic Mapping Tools) with 90-m-gridded SRTM (Shuttle Radar Topography Mission) topographic data (Kurt et al., 2019).

The length of the shortest line B2 is 1.9 km and the longest line B9 is 6.2 km. The length and the location of the lines were limited by the geographical features and practical aspects of the small boat operations. However, the lines were specifically chosen to be orientated north to south direction approximately perpendicular to the variations seen in the bathymetry data collected within the scope of the same project.

Data was acquired by external company SONARSEA using the research boat Curt Kosswig which belongs to Istanbul University Faculty of Aquatic Sciences (Figure 3.4).

Table 3.2 : Start of line (first shot point) and end of line (last shot point) coordinates of the profiles; latitude and longitude in decimal degrees.

Line Name	Start of Line		End of Line	
	Latitude	Longitude	Latitude	Longitude
Line 1_1 (B1)	40.72217283	30.20056266	40.7265625	30.20033233
Line 1_2 (B1)	40.70665016	30.20249266	40.72247233	30.20085566
Line 2_1 (B2)	40.721376	30.21632966	40.72073583	30.21652416
Line 2_2 (B2)	40.72146716	30.21652083	40.7092255	30.217537
Line 3 (B3)	40.7111535	30.2262395	40.72778683	30.22486983
Line 4 (B4)	40.726551	30.23462933	40.7052145	30.25173966
Line 5_1 (B5)	40.73146033	30.25323583	40.72579266	30.24760166
Line 5_2 (B5)	40.72760233	30.24882266	40.70603933	30.230448
Line 6 (B6)	40.70501366	30.24660283	40.73416333	30.26556416
Line 7 (B7)	40.7041495	30.25348166	40.73633866	30.275493
Line 8 (B8)	40.734648	30.28707283	40.70172766	30.26258933
Line 9 (B9)	40.7362245	30.27683866	40.6945275	30.2791195
Line 10 (B10)	40.73565316	30.29577983	40.700551	30.27299483
Line 11 (B11)	40.6991985	30.28248016	40.73201566	30.2989465
Line 12 (B12)	40.73019366	30.31338183	40.7010425	30.2958525
Line 13 (B13)	40.708233	30.313677	40.72193283	30.31317766

Figure 3.4 : Research boat Curt Kosswig (Istanbul University Faculty of Aquatic Sciences).

Equipment used during the acquisition of the “boomer” data are Geo-Spark 1000 Plus power supply, Geo-Source Boomer Plate and catamaran, Geo-Sense 8 Elements Mini-Streamer (AQ-2000 hydrophone) and Multi-Trace II 24-bit double-channel data acquisition system (Figure 3.5). A few of photographs taken during the preparation and deployment of the equipment are shown in Figure 3.6.

The best suitable acquisition parameters were chosen and decided upon based on the tests in the field prior to commencing the acquisition. Consequently, the data was

collected with 150-ms record length, 1-kHz sampling frequency (0.2-ms sample rate) and 500-ms shot interval with offsets X: -1 m and Y: -19.5 m.

Figure 3.5 : Equipment used for data acquisition; (a) Geo-Spark 1000 Plus power supply, (b) Geo-Source Boomer Plate and catamaran, (c) Geo-Sense 8 Elements Mini-Streamer (AQ-2000 hydrophone) and (d) Multi-Trace II 24-bit double channel data acquisition system.

Figure 3.6 : Preparation and deployment of the boomer sub-bottom profiler equipment (SONARSEA).

4. DATA PROCESSING

Seismic data processing can be described as the manipulation of seismic data by means of using computational techniques to obtain an enhanced image of the subsurface. Hence, data processing is important since correctly processed data leads to accurate interpretation of the subsurface structures.

For this study, data processing was carried out in Nezihi Canıtez Data Processing Laboratory located in Department of Geophysical Engineering of Istanbul Technical University using Paradigm® ECHOS® seismic processing software following the data processing flow chart shown in Figure 4.1. As shown in the flow chart, analyses and tests were performed to achieve the optimum parameterization for each processing step. Line 6 (B6), which is a mid-survey line, was chosen and mainly used for testing purposes along with Line 9 (B9) and Line 13 (B13).

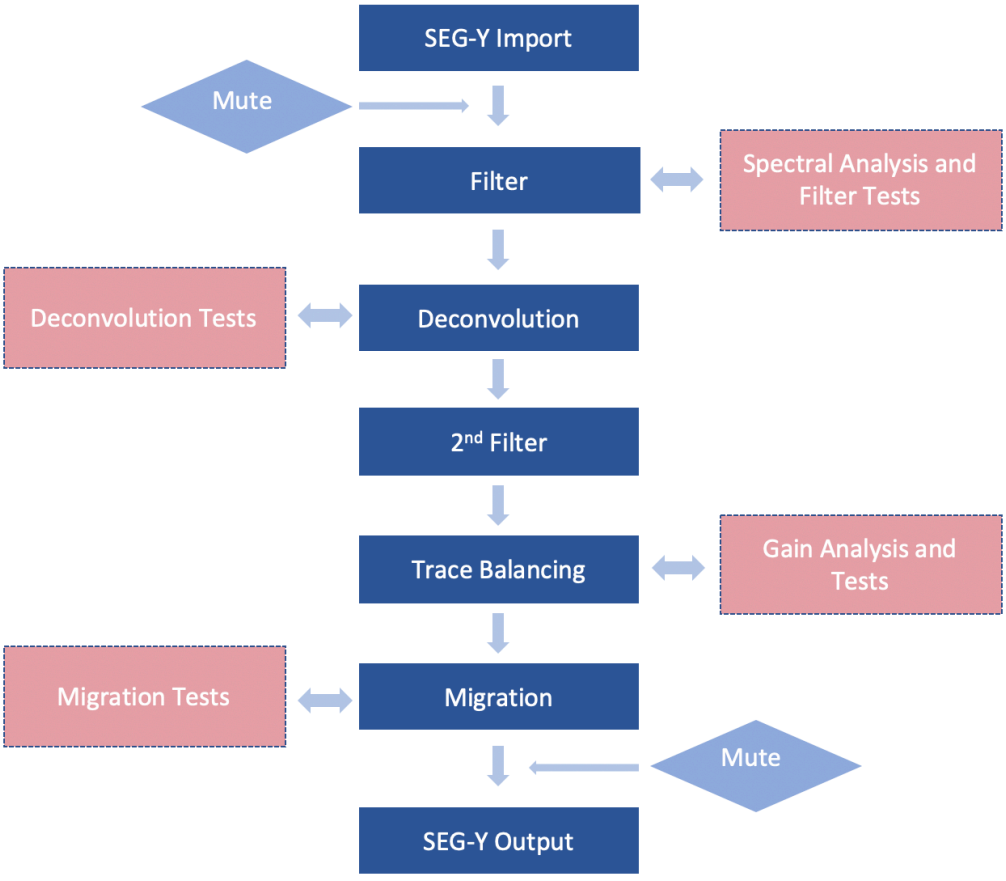

Figure 4.1 : Data processing flow chart.

Since the survey area was relatively small and the acquired data characteristics were quite similar, it was found suitable to use the same optimized parameters for every line which are presented in detail in the following sections.

4.1 Data Reading and Quality Control

The data was collected and recorded in SEG-Y format as per the configuration of the data acquisition equipment. The first step of the data processing was to convert the data into the internal disk data format so that the data was compatible with the software which was done using the SEG-Y Import/Export module of the Paradigm Software. For the visualization of the data during the data processing stages, dGB Earth Sciences' OpendTect seismic interpretation software was also utilized.

After the conversion, all raw data was visually reviewed using for quality control purposes. Consequently, Line 2_1 was deemed not to be processed as it was a very short line of approximately 70 shots (70 m) and contained several dead traces. The rest of the lines had no issues in terms of bad shots, dead traces, etc., and were passed on to the next processing stages.

Before moving onto the next step, a water column mute was also applied to each line to eliminate the high amplitude noise contamination and have a more suitable visualization of the data for comparison.

4.2 Spectral Analysis and Filtering

Main purpose of the seismic acquisition is to collect data which can represent the subsurface geology as close to the real image as possible, however, seismic data always contains both signal and noise where signal is used for interpretation of the subsurface and noise is the unwanted interference which might constrain and mislead the interpretation (Sengburg, 1983). Filtering the seismic data is a common practice for removing this undesired noise component. Therefore, finding the correct parameters for suppressing noise and enhancing resolution which is more related to signal-to-noise ratio than the sole frequency content, is important.

The Fourier transform is crucial to seismic data processing as it applies to most of the stages in processing. A seismic wavelet recorded by a receiver denotes a seismic trace for a specific location and this trace in a digital form can be described as a time series

of a discrete sum of sinusoids with a distinctive amplitude, frequency and phase components which are the products of the Fourier transform analysis (Yılmaz, 2001). Figure 4.1 illustrates the transformation from time to frequency and frequency to time domain with the application of forward and inverse Fourier transform, respectively.

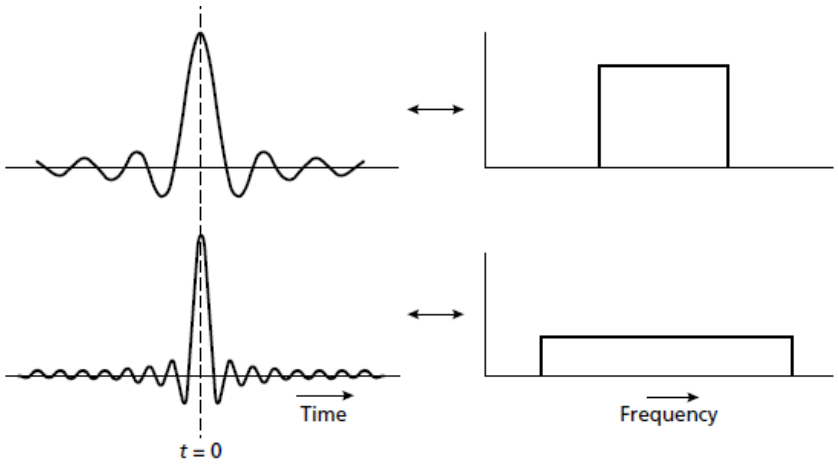

Figure 4.2 : Fourier transform pairs of waveforms approximating seismic pulses (Kearey, et al. 2002).

Amplitude spectrum which is a product of the Fourier Transform as explained above gives a good overview of the changes to the frequency content of the data before and after the application of each processing step. Therefore, the first step of data processing is to thoroughly examine the dataset along with the amplitude spectrum in order to identify and distinguish the noise from signal so that the correct adjustments can be applied to the data.

According to the amplitude spectra of Line 6 (B6), Line 9 (B9) and Line 13 (B13) shown in Figure 4.3, while the low end of the spectra is not as indicative as the high end, the frequency range to be preserved should lay between 0.4 kHz and 3 kHz. Spectrum of Line 6 also shows signs of more prominent noise content at both low and high frequencies where spectra of Line 9 and 13 are similar. A high-amplitude, low-frequency noise can also be observed at 40 Hz. This was thought to be an electrical leakage generated by the data acquisition instruments.

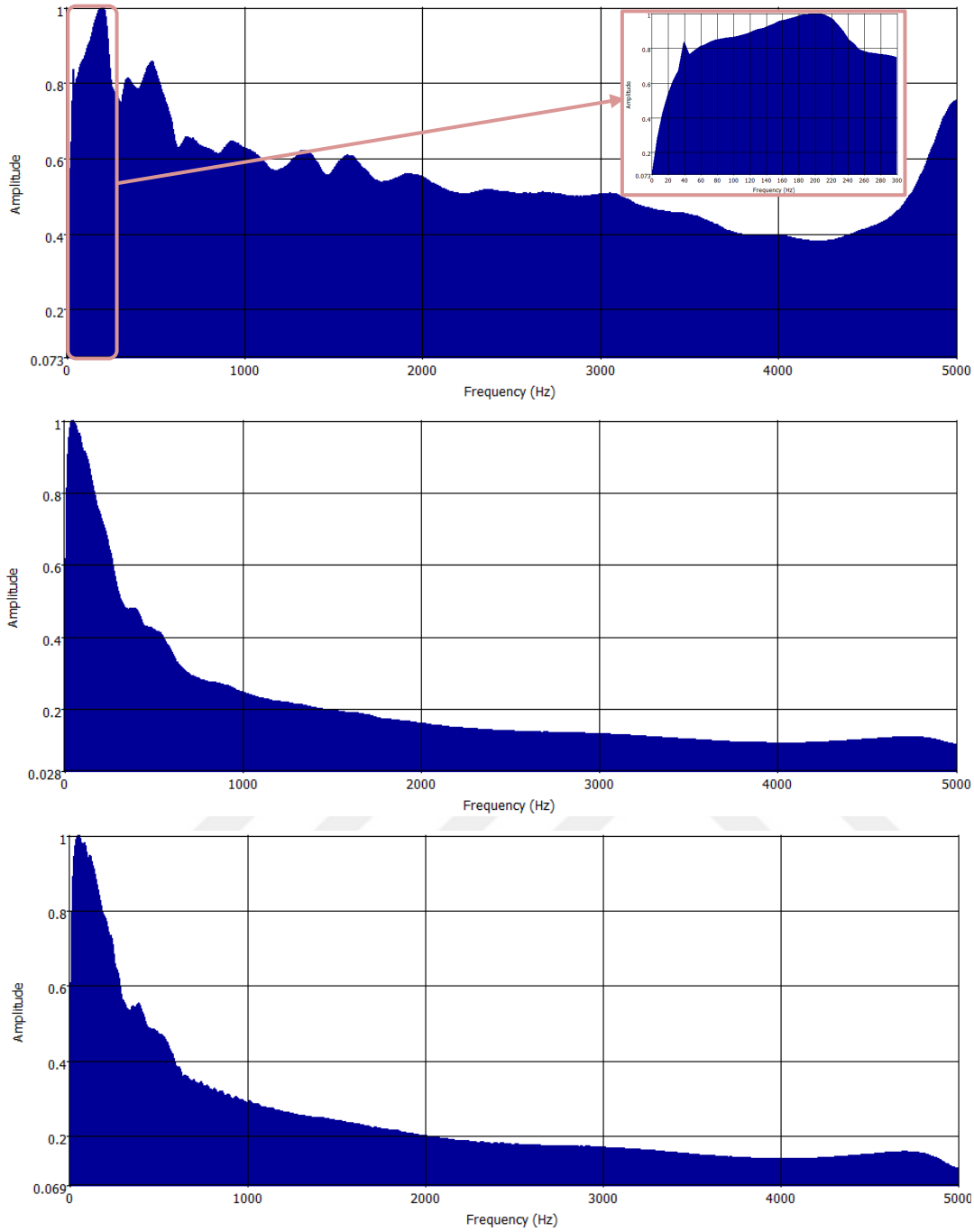

Figure 4.3 : Amplitude spectrum of Line 6 (B6) (top), 40-Hz noise more visible in horizontally zoomed display (top right); Line 9 (B9) (middle) and Line 13 (B13) (bottom).

In order to find the best filtering parameters suitable for the dataset in terms of noise attenuation while preserving the wide bandwidth and improving the resolution, several different tests were performed. For this study, band-pass filter approach was found more suitable.

In designing a band-pass filter, the aim is to keep a certain bandwidth with as little or no alterations as possible and to eliminate the rest as much as possible which can be

represented mathematically in terms of amplitude spectrum of a filter operator, where A is the amplitude, f_1 and f_2 are the cut-off frequencies, as follows (Yılmaz, 2001):

$$A(f) = \begin{cases} 1, & f_1 < f < f_2 \\ 0, & otherwise \end{cases} \tag{4.1}$$

Steep slopes in passband are result in undulations in the wavelet and the amplitude spectrum which is known as the Gibbs phenomenon caused by representing the wavelet with a finite number of Fourier coefficients, hence, a mild slope should be chosen to reduce the undulations (Bracewell, 1965 as cited in Yılmaz, 2001). Examples of different band-pass slopes can be seen in Figure 4.4.

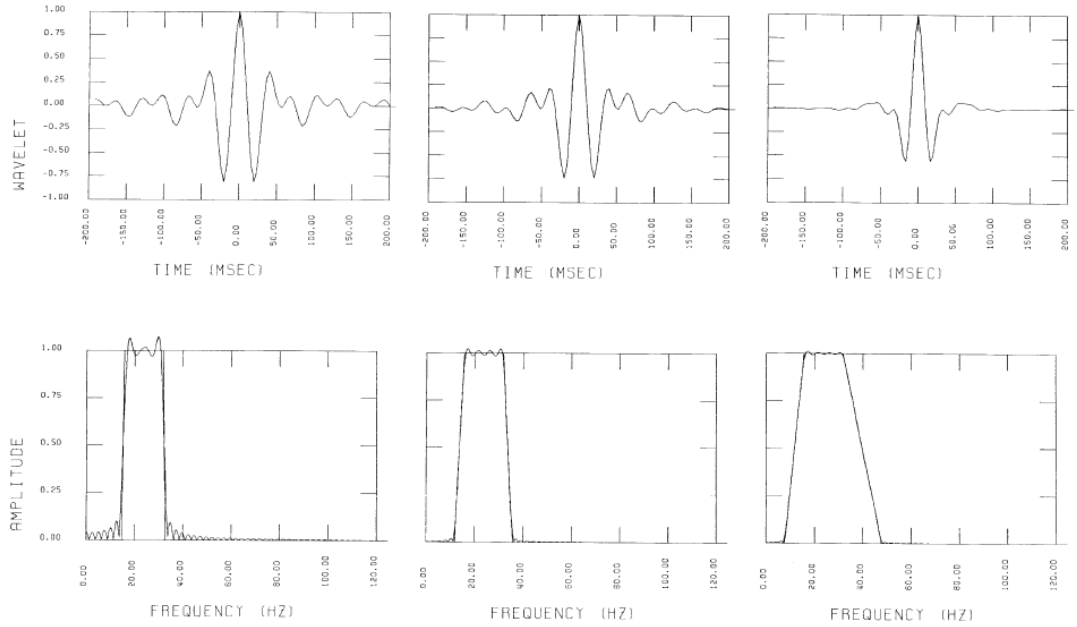

Figure 4.4 : Zero-phase wavelets (top) and their respective amplitude spectra (bottom) (Yılmaz, 2001).

Band-pass filters require four corner frequencies to define trapezoidal passband. First parameter tested was these corner frequencies keeping all other parameters the same and the second parameter to test was the filter length. Finally, the testing was completed by comparing the effects of smoothing operators. Each test parameters and final filter parameters decided to be applied to the data are given in Table 4.1.

Test 02 also included an additional notch filter applied to eradicate the 40 Hz noise which is shown in Figure 4.3 (top) and all the following tests were conducted keeping the notch filter as default. It should also be noted that the notch filter application was exclusive for Line 6 (B6).

Table 4.1 : Filter test parameters; BP=band pass, HP=high pass, Min=minimum, HANN=hanning, HAMM=hamming, COS=cosine, TRI=triangular. Test 16 was the final optimized filter parameters used ("*" indicates the final filter parameters).

Test No.	Type	Length (ms)	Phase	Taper	Filter Corner Frequencies (Hz)			
					f1	f2	f3	f4
01	BP	15	Min	HANN	80	120	1400	1700
02	BP	15	Min	HANN	80	120	1400	1700
03	HP	15	Min	HANN	80	120	-	-
04	BP	15	Min	HANN	80	120	2800	3150
05	BP	15	Min	HANN	80	120	960	1080
06	BP	5	Min	HANN	80	120	2800	3150
07	BP	10	Min	HANN	80	120	2800	3150
08	BP	20	Min	HANN	80	120	2800	3150
09	BP	40	Min	HANN	80	120	2800	3150
10	BP	50	Min	HANN	80	120	2800	3150
11	BP	5	Min	HAMM	80	120	2800	3150
12	BP	5	Min	COS	80	120	2800	3150
13	BP	5	Min	TRI	80	120	2800	3150
14	BP	5	Zero	HANN	80	120	2800	3150
15	BP	5	Min	HANN	80	120	2800	3150
16*	BP	5	Min	HANN	450	480	2800	3150
17	BP	5	Min	HANN	450	480	4000	5000

Results of Test 01 and 02 along with the raw data and their relevant amplitude spectra are shown in Figure 4.5. Both tests have the exact same filter settings except Test 02 having an additional notch filter as mentioned earlier. Although the band-pass range in Test 01 covered 40 Hz in the cut-off range, amplitude spectra still showed some left-over contamination at that frequency. Thus, this was the reason why an additional notch filter needed.

Figure 4.6 shows the results of Tests 03, 04 and 05. These three tests were performed to see the effects of different cut frequencies at the high end of the spectrum. And the results show that frequency corner pair of 2.8 kHz and 3.15 kHz is a more suitable as it maintains the wide spectrum. Consequently, these were kept as final high cut off frequencies.

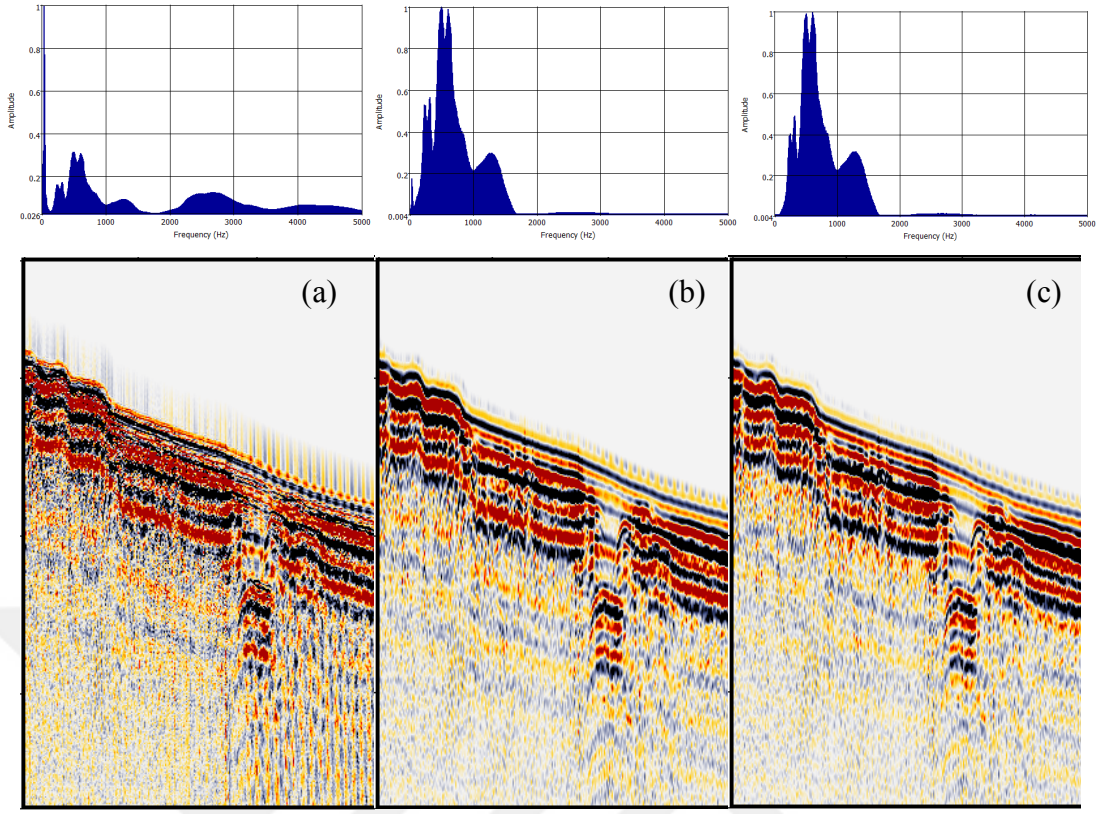

Figure 4.5 : Comparison of (a) raw data, (b) Test 01: band-pass filter and (c) Test 02: band-pass filter plus notch filter, amplitude spectra on top.

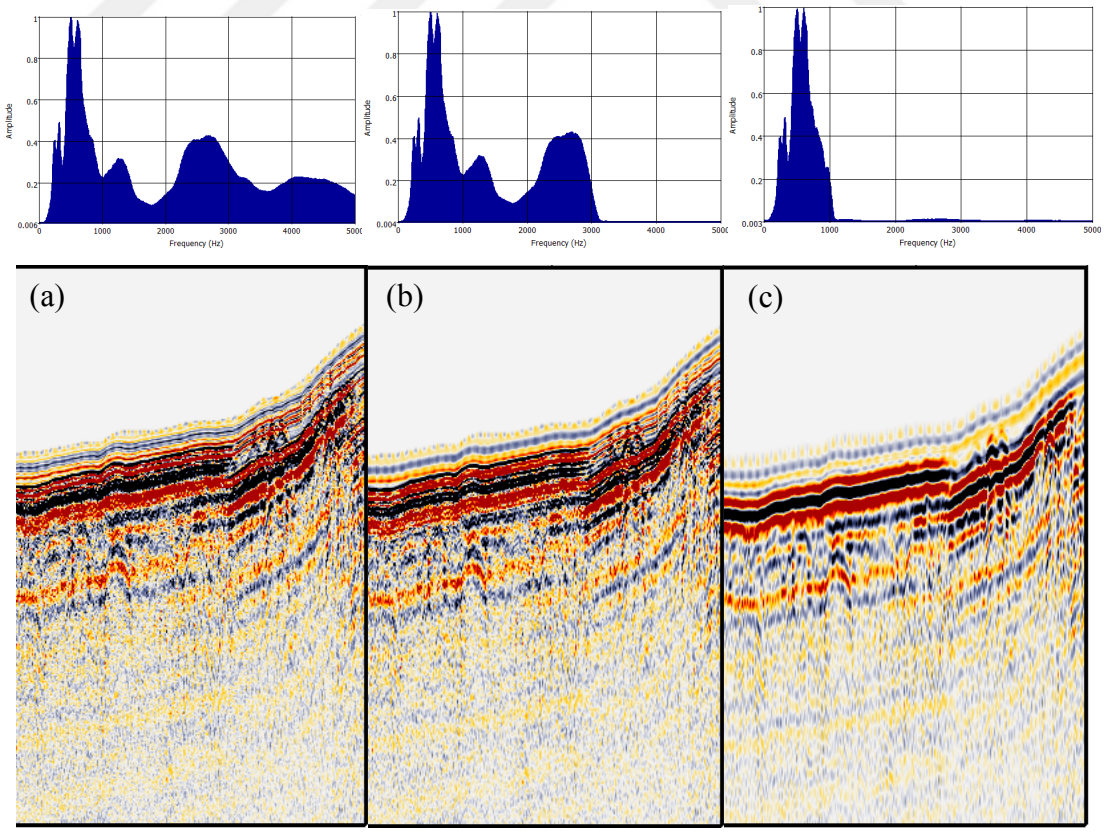

Figure 4.6 : Comparison of corner frequencies; (a) Test 03, (b) Test 04 and (c) Test 05, amplitude spectra on top.

It is the most ideal to have the designed and actual spectra equal and the filter operator narrow but more difference is observed between the real and desired spectra if the operator length is too short (Yılmaz, 2001). As shown in Figure 4.7, longer filter length means the designed and actual spectra are similar, however, the length of the operator is limited by the nearly zero coefficients added to the operator (Yılmaz, 2001).

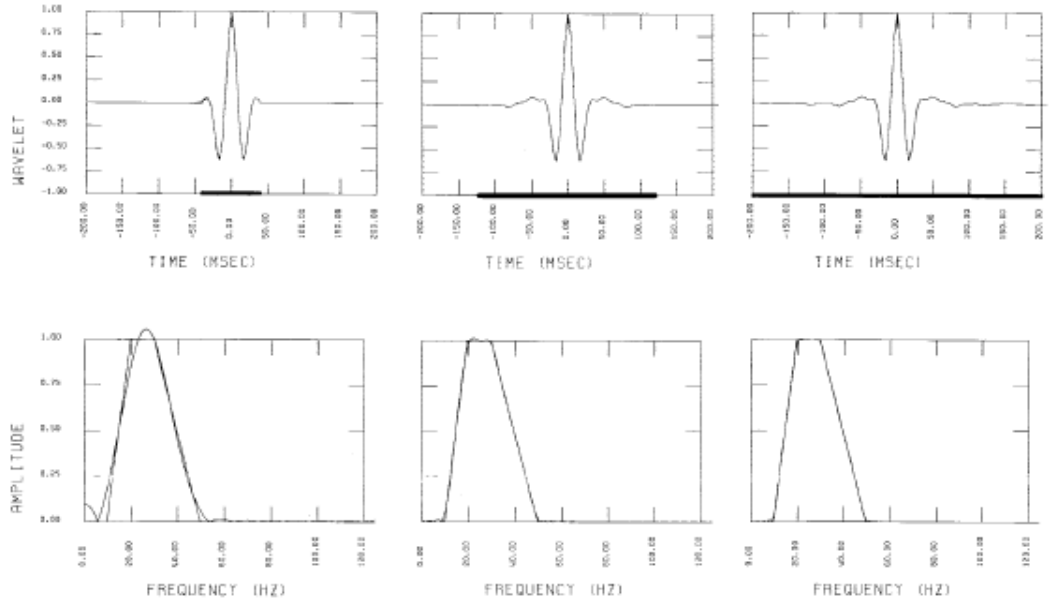

Figure 4.7 : Filter operator lengths (top) and their associated trapezoidal amplitude spectra (bottom) (Yılmaz, 2001).

Effects of applying different operator lengths can be seen in Figure 4.8. Although, only subtle differences are visible mainly in the amplitude spectra, filter length of 5 ms seems to flatten the areas outside the passband more effectively while preserving the amplitudes slightly more in the higher frequencies. Additionally, frequency bandwidth also dictates the effective length of the filter as they are inversely proportional (Yılmaz, 2001). Thus, since the bandwidth of the dataset spans up to 5 kHz, using a relatively shorter operator length seemed like a reasonable choice for this study. Therefore, 5 ms was decided as the final filter length.

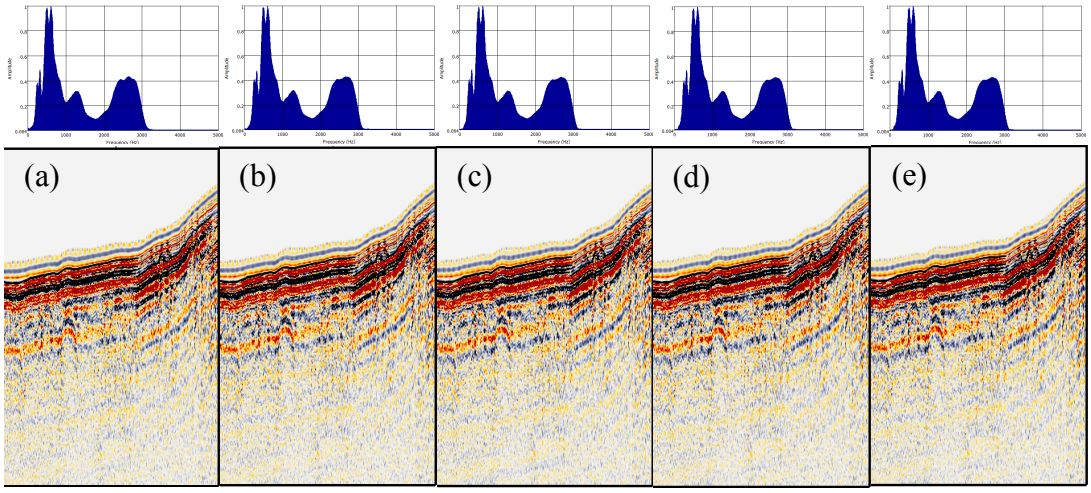

Figure 4.8 : Comparison of filter (operator) lengths; (a) Test 06, (b) Test 07, (c) Test 08, (d) Test 09 and (e) Test 10, associated amplitude spectra on top.

A taper should also be applied at the corner frequencies since the Fourier transform exists only for continuous functions (Bracewell, 1965 as cited in Yılmaz, 2001). ECHOS software offers four different tapering options as listed below and taper coefficients are calculated as follows:

- Hanning: $0.5 + 0.5\cos(A), 0 < A < \pi$;
- Hamming: $0.54 + 0.46\cos(A), 0 < A < \pi$;
- Cosine: $\cos(A), 0 < A < \frac{\pi}{2}$ and
- "Triangular" operates as a linear interpolator.

Taper test results are presented in Figure 4.9. Again, test results do not show significant differences apart from ripples at the higher end of the spectrum on Test 14 for which the linear interpolation taper used. Wavy pattern is also noticeable right above the water column in the data. Consequently, the Hanning taper was chosen to use as final smoothing parameter.

As per the wide frequency range of high-resolution seismic profiling, some of the noise content might be confined in the actual signal frequency range which would be challenging to suppress or to completely eliminate since it would compromise the preservation of the signal frequencies (Houlding, 1994 as cited in Marino et al. 2013). An example of this type of noise (spiking) can be seen in Figure 4.10. Individual spectral analysis showed that the noise is at around 1.3 kHz which falls in the native frequency range of the acquired data. In this particular case, which only affects Line

10 (B10), Line 11 (B11) and Line 12 (B12), the spiking was deemed negligible since it does not significantly affect the quality of interpretation in the later stage.

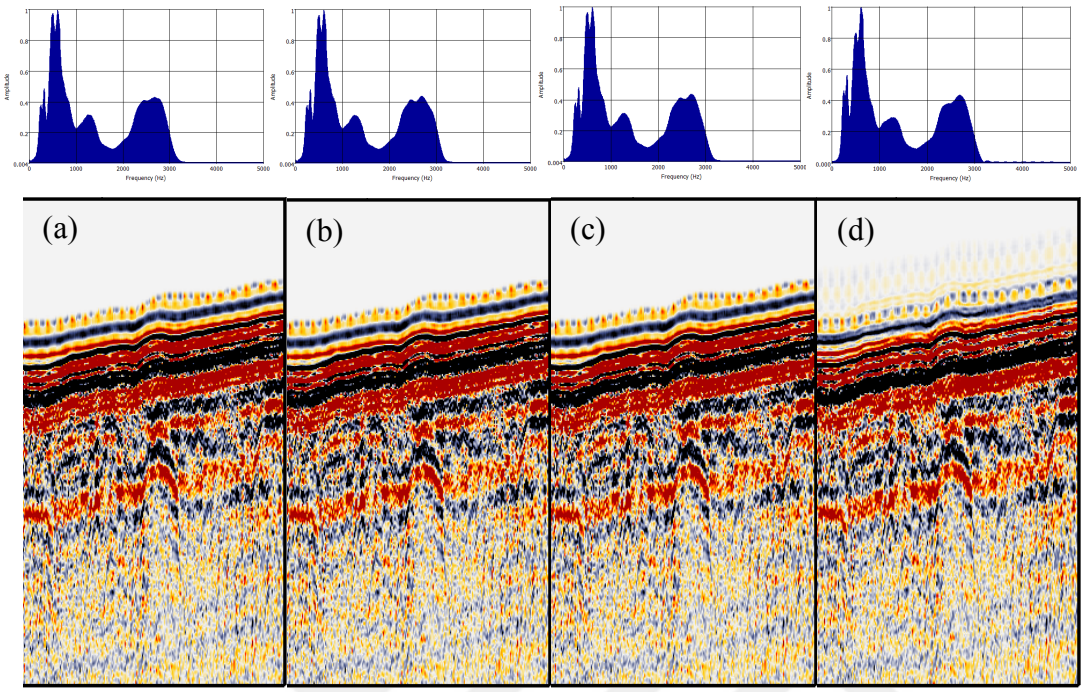

Figure 4.9 : Comparison of taper operators; (a) Test 11, (b) Test 12, (c) Test 13 and (d) Test 14, amplitude spectra on top.

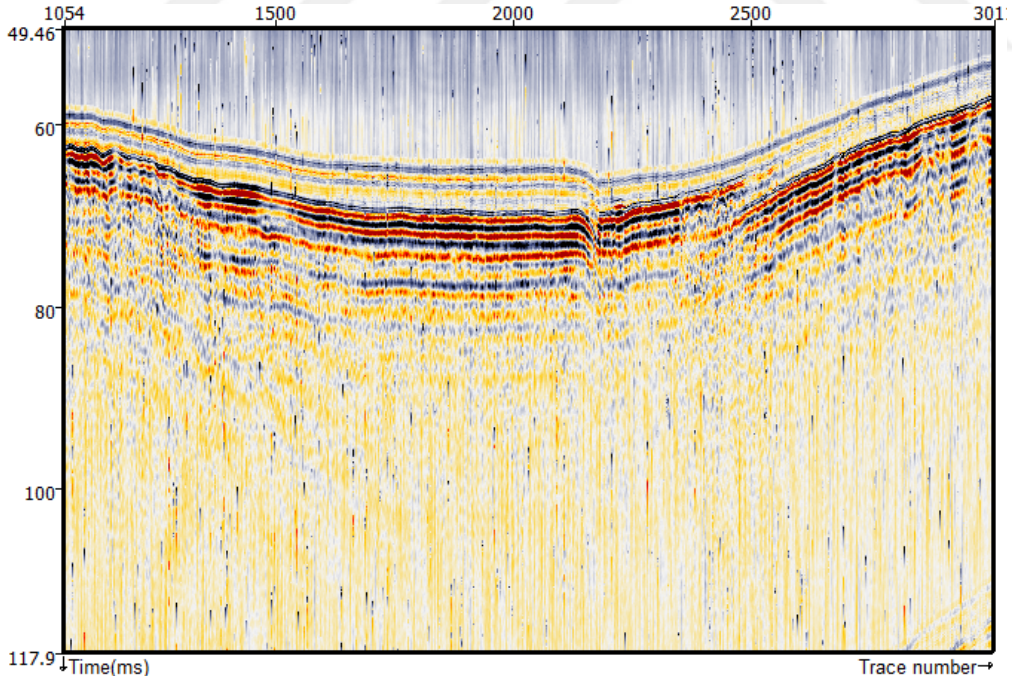

Figure 4.10 : High-frequency random spiking on Line 11 (B11) raw data.

Finally, the raw data and filtered data using the final optimized parameters are shown in Figure 4.11.

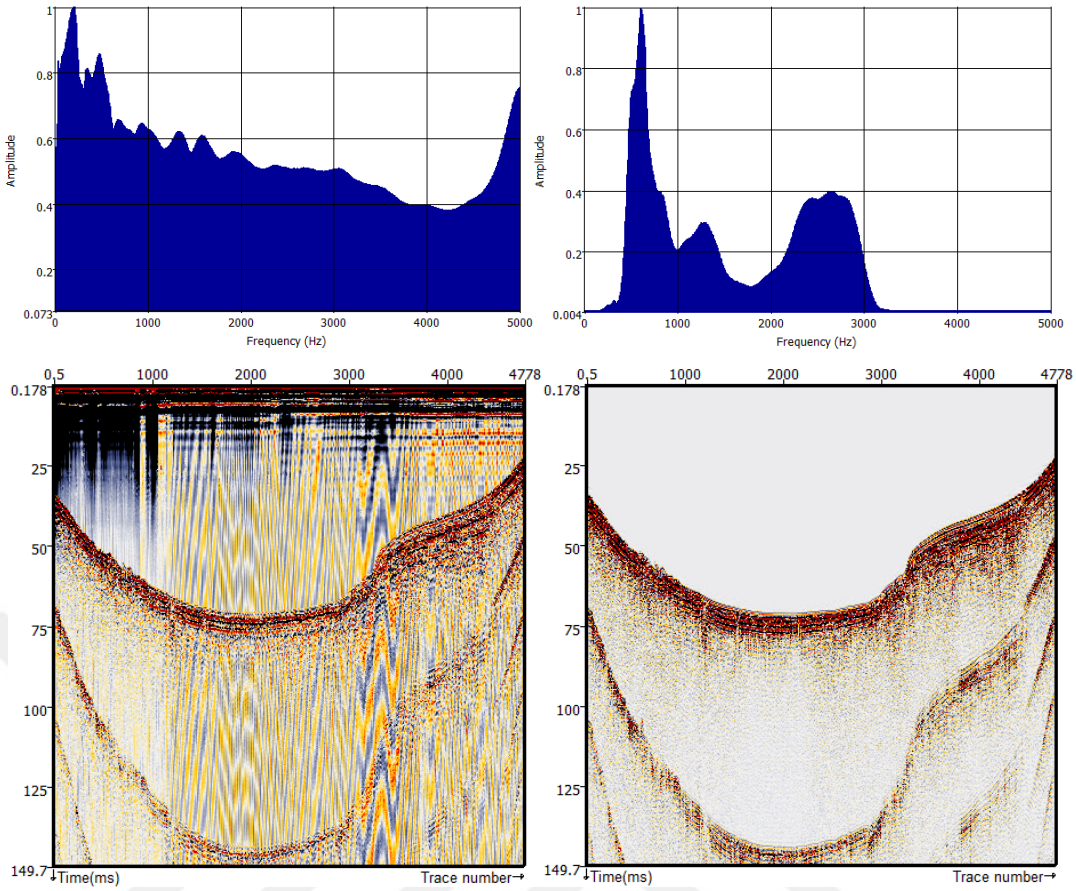

Figure 4.11 : Line 6 (B6), before (left) and after (right) filter application, amplitude spectra on top.

4.3 Deconvolution

A seismic trace or a seismogram is a product of the response of the subsurface and a recording system to a seismic source wavelet. Therefore, the seismic trace can be described as the convolution of the source pulse with the reflectivity function which is made up of series of reflection coefficients or spikes relevant to each subsurface geological boundary plus noise as illustrated in Figure 4.12 (Wail and Shuhail, 2011).

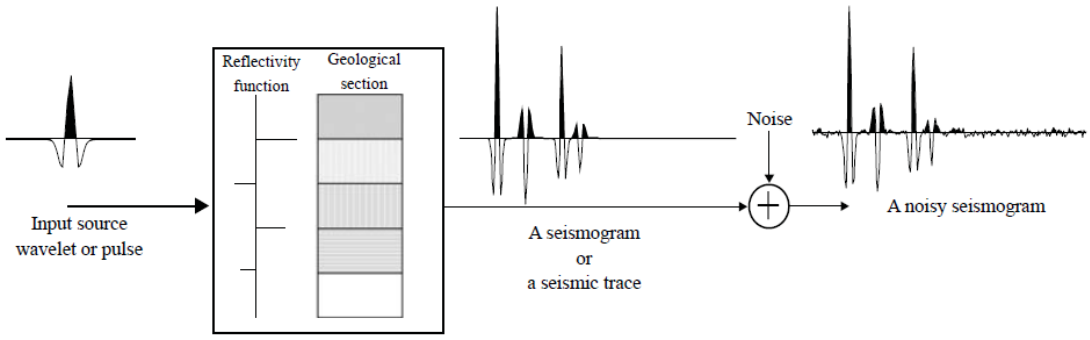

Figure 4.12 : Convolution seismic data model in terms of producing a seismic trace (Wail and Shuhail, 2011).

Deconvolution is the inverse convolution process of removing noise and subsequently determining and eliminating the input source to leave only the reflectivity function from which the reflection coefficients are extracted (Wail and Shuhail, 2011).

As a consequence of performing frequency filtering on seismic data, the seismic data is smoothed and its resolution is compromised due to the loss of some of its wider frequency band, hence, deconvolution, also help improve the amplitude spectrum and sharpen the seismic events regaining some of the lost frequencies (Wail and Shuhail, 2011).

There are two main types of deconvolution methods; spiking deconvolution and predictive deconvolution. Spiking deconvolution is suitable for increasing vertical resolution where predictive deconvolution is useful for removing multiple reflections. Fundamentally, spiking deconvolution is a form of predictive deconvolution where the prediction lag is equal to the sampling rate which is 2 ms in most conventional seismic data. In this study, the dataset has a sampling rate of 0.2 ms, therefore, it was not possible to test and consequently perform a spiking deconvolution due to the design of the software binary module which requires the prediction lag in integer "points" (2 ms=1 point). Thus, only the predictive deconvolution method was tested and consequently performed on the data.

In practice, predictive deconvolution requires two important parameters; operator length of the prediction filter which is the first transient zone length of autocorrelation wavelet in time and the prediction lag which is either the first or second zero-crossing time of the of the autocorrelation wavelet (Yılmaz, 2001).

By examining an autocorrelation trace from Line 13 (B13), the suitable operator length, the first zero-crossing and the second zero-crossing time were determined to be 12 ms, 0.4 ms and 1.1 ms, respectively. Based on these values, several test parameters were chosen for both the operator length and the prediction lag which are given in Table 4.2.

Table 4.2 : Deconvolution test parameters ("*" indicates the final deconvolution parameters).

Test No.	Operator Length (ms)	Prediction Lag (ms)
01	12	0.4
02*	24	0.4
03	48	0.4
04	96	0.4
05	24	1.1
06	24	0.8

Operator length test results are presented in Figure 4.13. As the operator length increases the amplitude spectrum becomes flatter which is desirable, but the data looks more jittery. Thus, 24 ms operator length was found more suitable as it flattens the amplitude spectrum while keeping the horizons sharper at the same time.

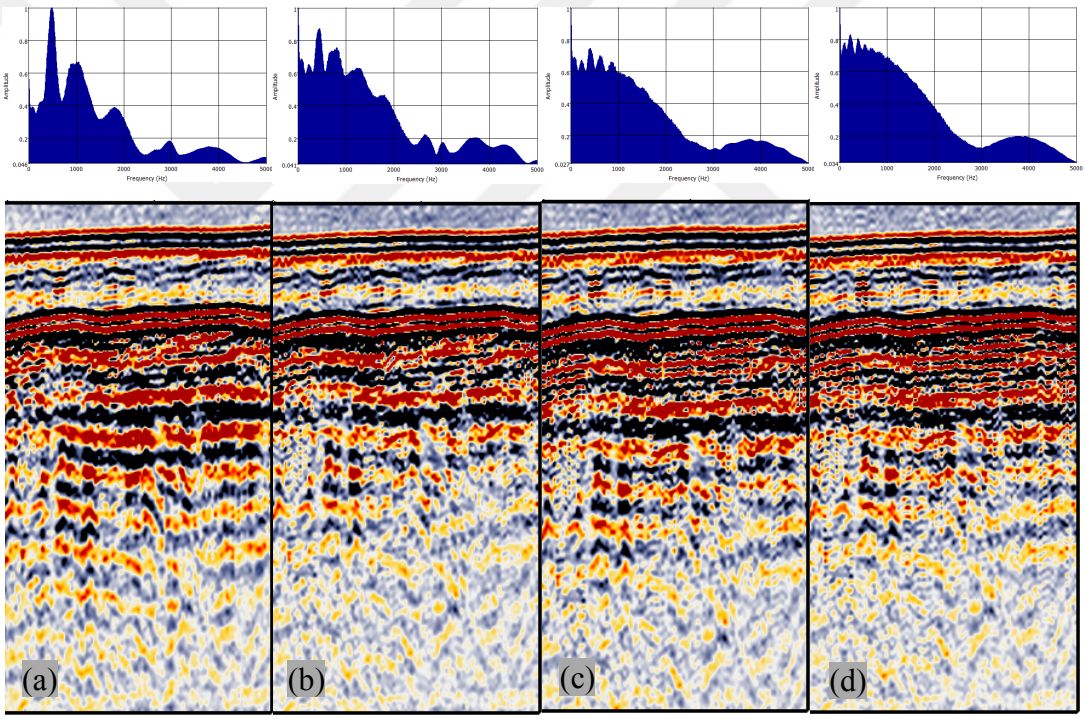

Figure 4.13 : Comparison of operator length; (a) Test 01, (b) Test 02, (c)Test 03 and (d) Test 04, amplitude spectra on top.

In Figure 4.14, results of different prediction gaps with the same operator length of 24 ms are shown and for the same reasons explained above, prediction lag of 0.4 ms was decided to be the right parameter.

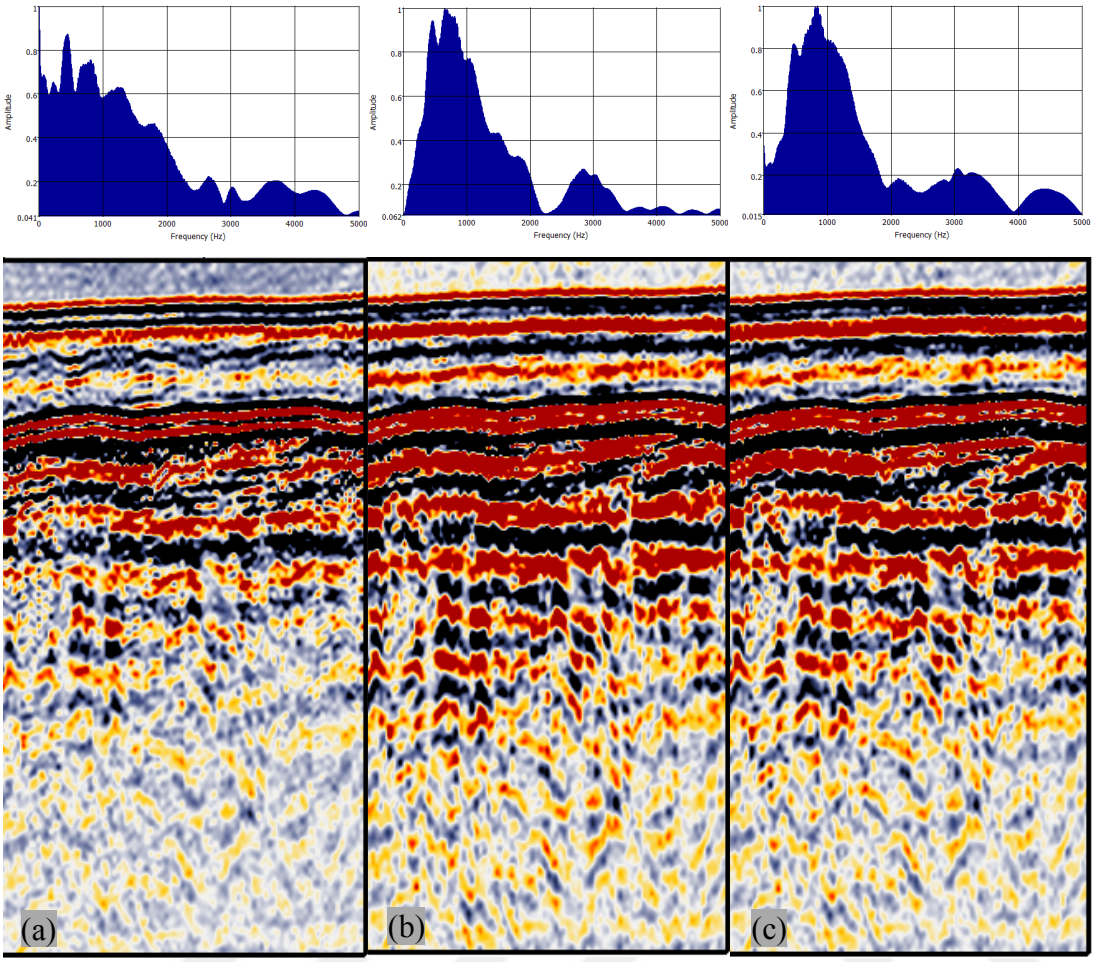

Figure 4.14 : Comparison of prediction lag (gap length); (a) Test 02, (b) Test 05 and (c) Test 06, amplitude spectra on top.

Pre- and post-deconvolution data are shown in Figure 4.15. Multiple reflections are not eliminated, however suppressed; the vertical resolution is increased as the frequencies specifically above 1 kHz are regained. Since the deconvolution process introduces noise, a secondary filter was also applied to the data after deconvolution (Figure 4.15).

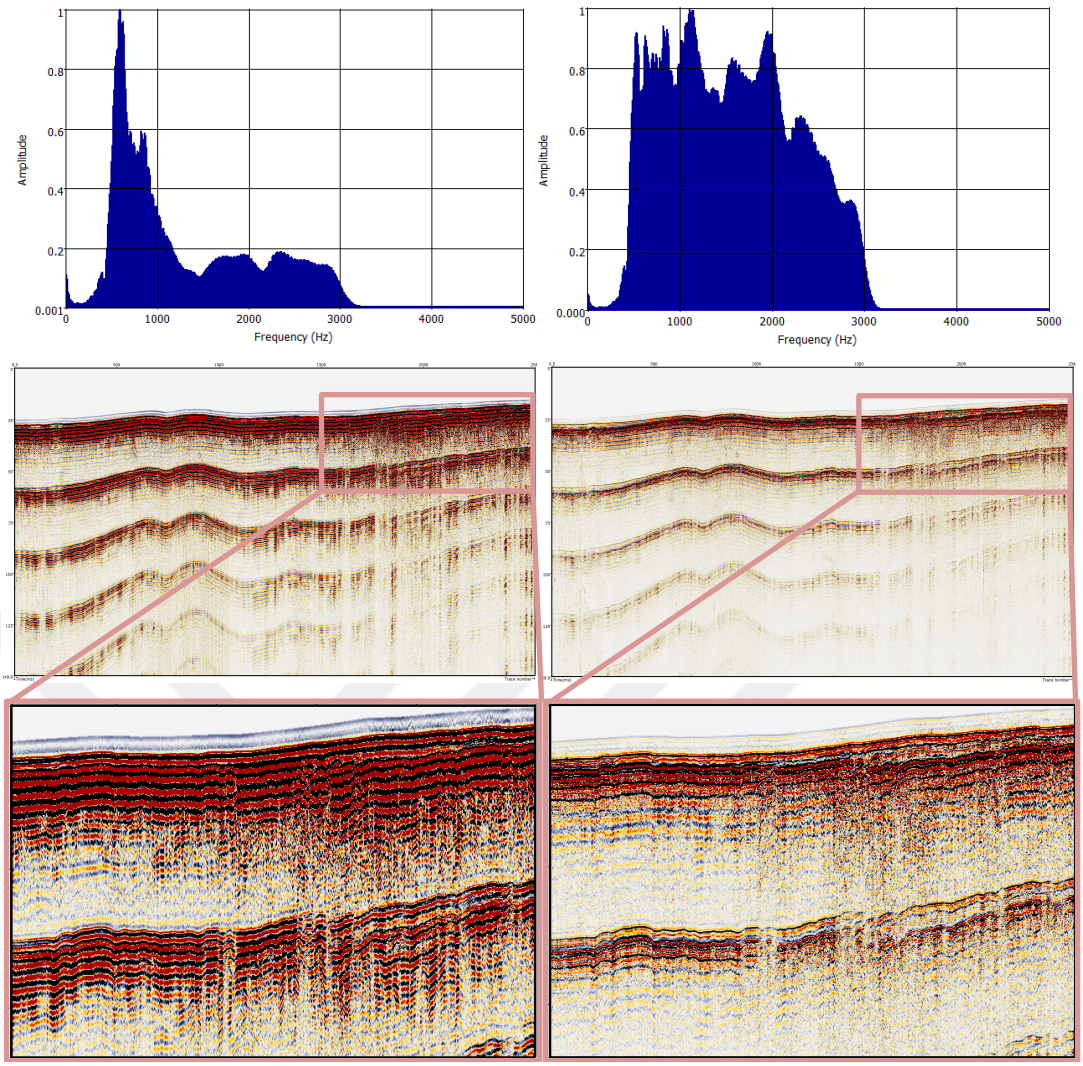

Figure 4.15 : Line 13 (B13), before (left) and after (right) deconvolution (post-deconvolution BP filter also applied), amplitude spectra on top.

4.4 Trace Balancing

Trace balancing method was used to adjust the gain properties of the data after deconvolution to improve the displays in order to have a better image quality. Conventional gain applications alter the trace amplitudes by a function $g(t)$ in a time-dependent fashion while trace balancing, which is commonly used right after deconvolution, is a time-independent scaling method based on rms amplitudes where the balance factor is defined as the ratio of the desired rms to the rms amplitude that is computed from a specified time window (Yılmaz, 2001).

Scalars are calculated from the amplitude of the trace samples within a given time window with which it multiplies the samples of each input trace. Scalars that multiply points on the trace between the gate midpoints are derived by linear interpolation.

Average amplitude is computed by summing the absolute value of all data samples within the gate and dividing by the number of nonzero sample points which can be defined by the user as given in equation 4.2:

$$Average\ Amplitude = \sum_{Beginning\ of\ Gate}^{End\ of\ Gate} \frac{|trace(T)|}{N} \tag{4.2}$$

where T is the sample time and N is the number of nonzero samples within a gate. The equalization scalar is then calculated by the equation 4.3:

$$Equalization\ Scalar = \frac{Scaling\ Factor}{Average\ Amplitude} \tag{4.3}$$

where $Scaling\ Factor$ is a user-defined value.

Testing with different start and end times (gate start and gate end) was performed on Line 6 (B6) using the same scalar factor of 1. Testing parameters are given in Table 4.3 and test results before and after Test 01, Test 02 and Test 03 (2) are presented in Figures 4.16, 4.17 and 4.18, respectively.

Table 4.3 : Gain test parameters, Scaling Factor=1 for all tests ("*" indicates the final gain parameters).

Test No.	Gate Start (ms)	Gate End (ms)
01	70	90
02	30	90
03*	15	100

Additionally, in Figure 4.19, a closer look at the results are shown. There are only subtle differences between the results of Test 02 and Test 03, however, latter shows that the amplitudes are balanced and refined better serving for the purpose and the focus of interpretation; water-bottom is more defined especially in the middle part of the section and areas immediately below and near water-bottom are clearer. Thus, Test 03 parameters were accepted as final gain balance application parameters.

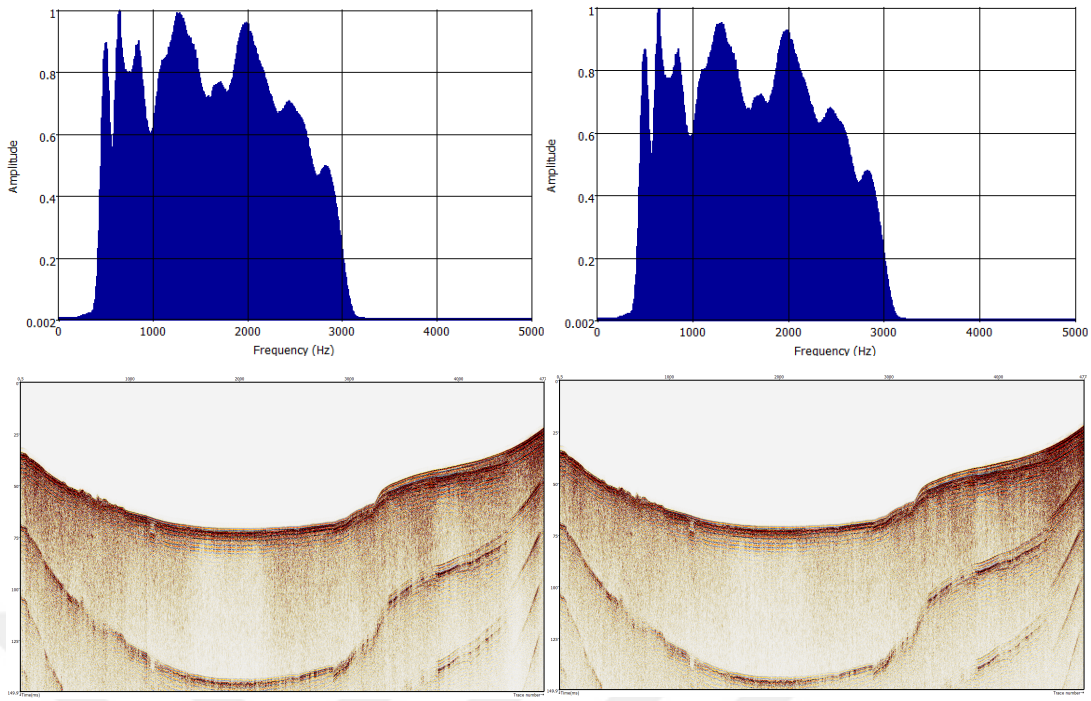

Figure 4.16 : Line 6 (B6), before (left) and after (right) gain balance (Test 01), amplitude spectra on top.

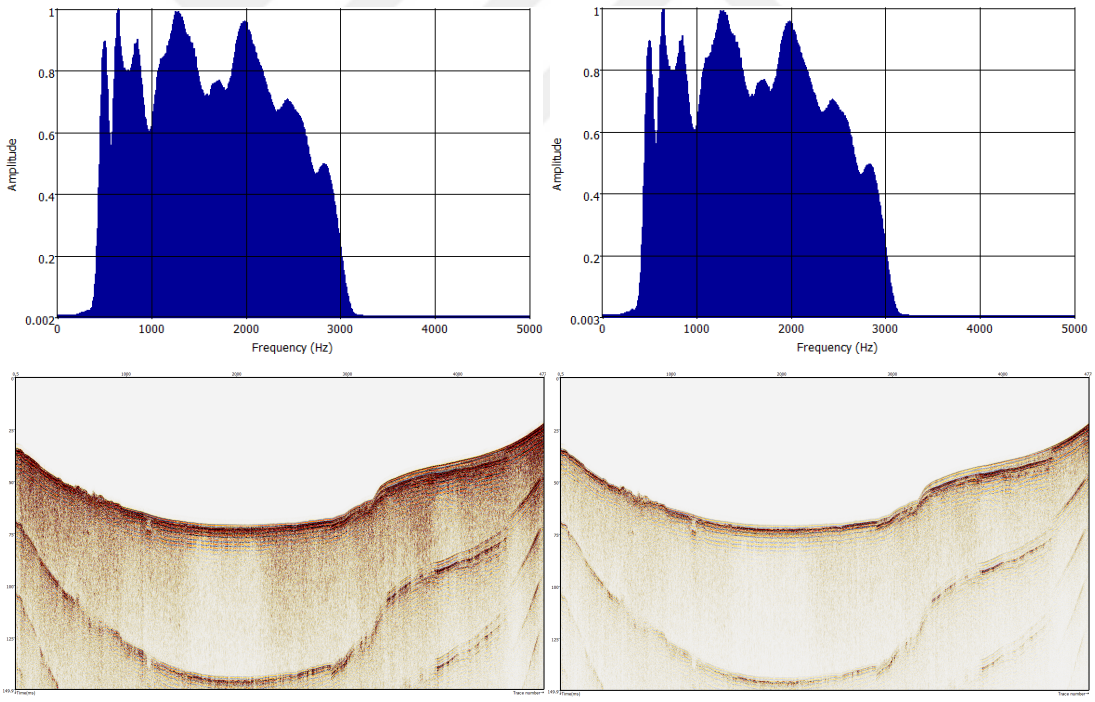

Figure 4.17 : Line 6 (B6), before (left) and after (right) gain balance (Test 02), amplitude spectra on top.

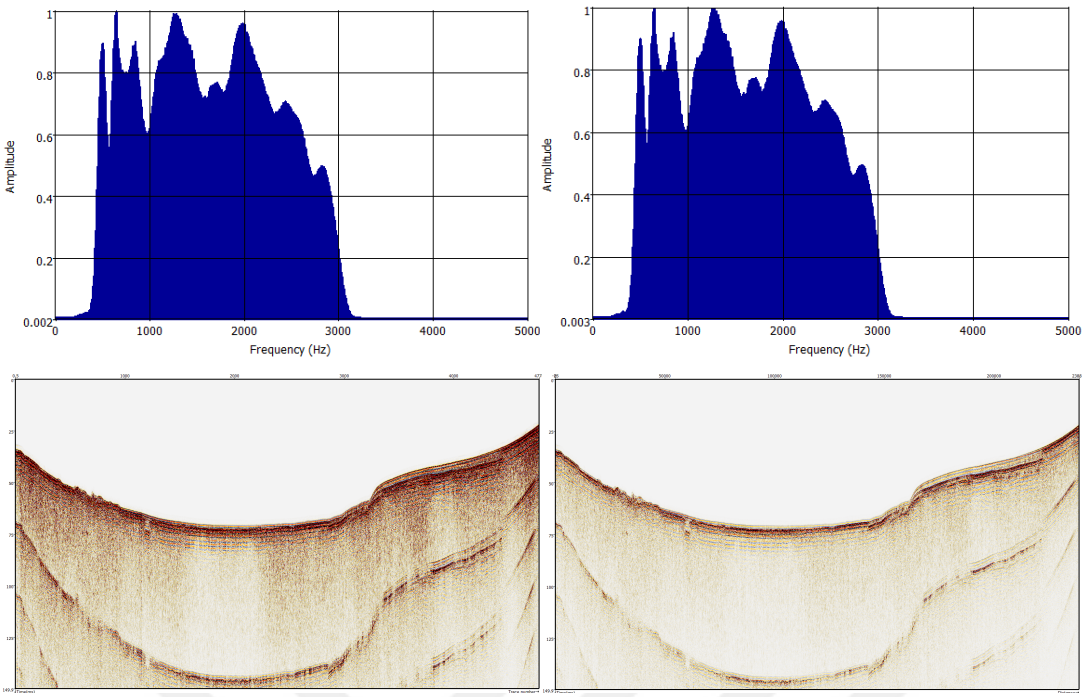

Figure 4.18 : Line 6 (B6), before (left) and after (right) gain balance (Test 03), amplitude spectra on top.

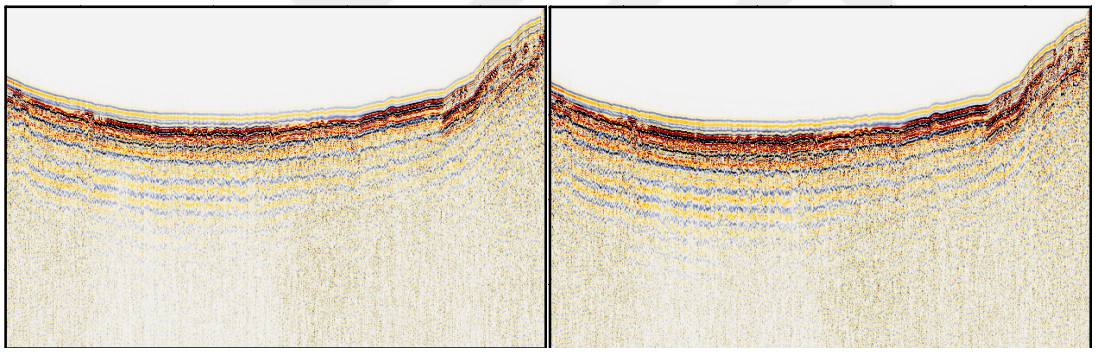

Figure 4.19 : Line 6 (B6), zoomed display of Test 02 (left) vs. Test 03 (right).

4.5 Migration

The point from where the seismic waves are reflected can only be considered directly underneath the surface in an ideal situation of where the reflector layer is horizontal, however, in reality, this is not often the case due to the complex structural nature of the subsurface. Seismic migration is the process of restructuring a seismic section to carry these reflection events, i.e. dipping layers, to their actual locations at the correct reflection times (Kearey et al., 2002).

True dip angle of a dipping layer is always greater than the apparent dip angle seen on seismic section (Yılmaz, 2001; Wail and Shuhail, 2011). Figure 4.21 shows the

relation between the angle of dipping of the apparent and true locations of a dipping layer.

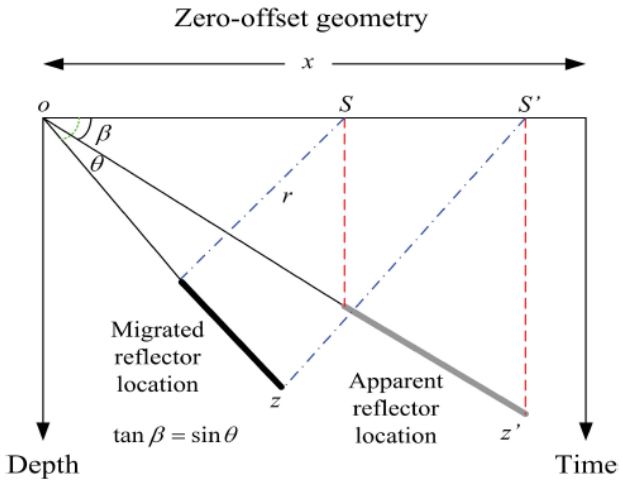

Figure 4.20 : After migration, dip angle of the reflector increases and it gets shortened (Wail and Shuhail, 2011).

For a reflector with a true dipping angle of θ and for a wavefield propagating from distance x down to the reflector, the zero-offset two-way travel time is given by:

$$t = \frac{2r}{c} \tag{4.4}$$

where c is the velocity of the propagating wave (which is assumed to be constant) and r is the wavefield path length which is equal to $r = x \sin\theta$. In order to compare the true and apparent dip angles, the travel time must be converted to depth calculating the minimum two-way travel time via equation:

$$t_0 = \frac{2z}{c} \tag{4.5}$$

where, the depth of the dipping layer, $z = x \sin\theta$ in the unmigrated depth section. For a reflector with an apparent dip angle β, the relation becomes:

$$\tan\beta = \sin\theta \tag{4.6}$$

which shows that the apparent dip angle is always less than true dip angle (Wail and Shuhail, 2011).

On a seismic section a point reflector is recorded as a diffraction hyperbola, and migration process adds the amplitudes along the hyperbolic curve and collapses the event at the apex of the hyperbola (Kearey et al., 2002). Diffraction migration is illustrated in Figure 4.20.

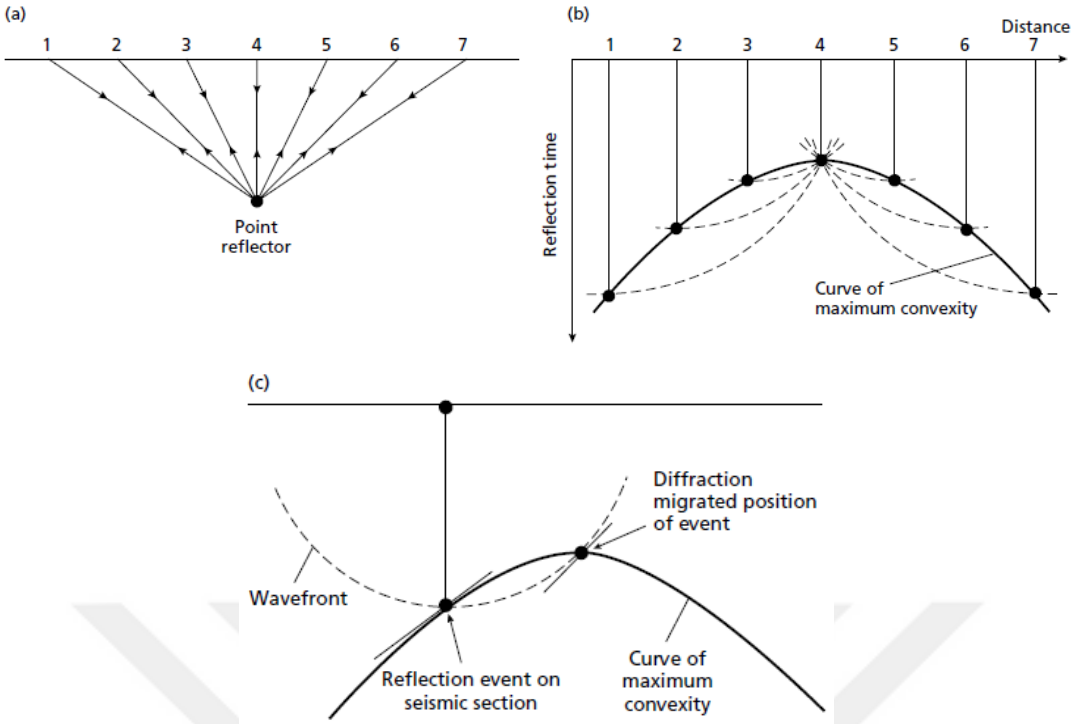

Figure 4.21 : (a) Reflection paths from a point scatterer. (b) Arrival times of reflections and their migration back to position of point scatterer. (c) A specific reflection event is tangential to the curve of maximum convexity and the migrated position of the event is at the intersection of the wave-front with the apex of the curve (Kearey et al., 2002).

Migration can be applied to pre-stack and post-stack data within which can be divided into groups of time and depth migration. The three main migration techniques are Kirchhoff migration, Frequency-wavenumber (Stolt) migration and finite-difference migration.

As the single-source, single-receiver dataset in hand can be considered as a single-trace section or pseudo-post-stack section, post-stack time migration method with finite-difference algorithm was found to be best suitable method for our study. Finite-difference migration algorithm is based on propagating a wave field using finite-difference approximations to the wave equation with a time frame implementation reference to a vertically upwards traveling wave (Claerbout and Johnson 1971; Claerbout and Doherty 1972).

Method requires a time-rms velocity pairs. Since it was not possible to perform a conventional velocity analysis for our dataset, a velocity file (several for testing purposes) was created based on the average CTD (Conductivity, Temperature, Depth) measurements, which is 1459 m/s, taken daily during the survey for accurate speed of sound readings in the water column. Then the interval velocities to be used for

migration are calculated from the time-rms velocity table that is constructed at increments of TAU, the migration layer thickness in two-way travel time (TWT) which is user-specified. The velocities that correspond to the TAU layer time increments are then linearly interpolated which means that each time layer (TAU) has a different interval velocity.

Migration process also requires the subsurface distance increment between the between common depth point (CDP) traces which is 1 m. Another parameter to be used is the maximum dip value for each section (line) which was determined by finding the most dipping events on a section and calculating the dip in ms/trace. Maximum dip was determined to be 0.17 ms/trace for Line 9 (B9) which was subject to migration tests.

To obtain the most fitting parameters for migration process, several tests were conducted with different set of velocity files and TWT layer thickness (TAU) values which are given in Table 4.4 and 4.5, respectively.

Table 4.4 : RMS velocities used in migration test process ("*" indicates the final velocities).

Time	RMS Velocities (m/s)					
(ms)	1	2	3	4	5	6*
0	1459	1400	1350	1300	1450	1400
50	1460	1450	1400	1335	1450	1450
100	1480	1480	1480	1375	1500	1500
150	1500	1550	1550	1400	1700	1700

Table 4.5 : Migration test parameters ("*" indicates the final gain parameters).

Test No.	tau (ms)	Velocity
01	2	01
02	12	01
03	30	01
04	2	02
05	12	02
06	30	02
07	20	03
08	20	04
09	20	05
10*	32	06

The effects of using different TAU values are shown in Figure 4.22. TAU values of 2, 12 and 30 are shown with Test 01, 02 and 03, respectively.

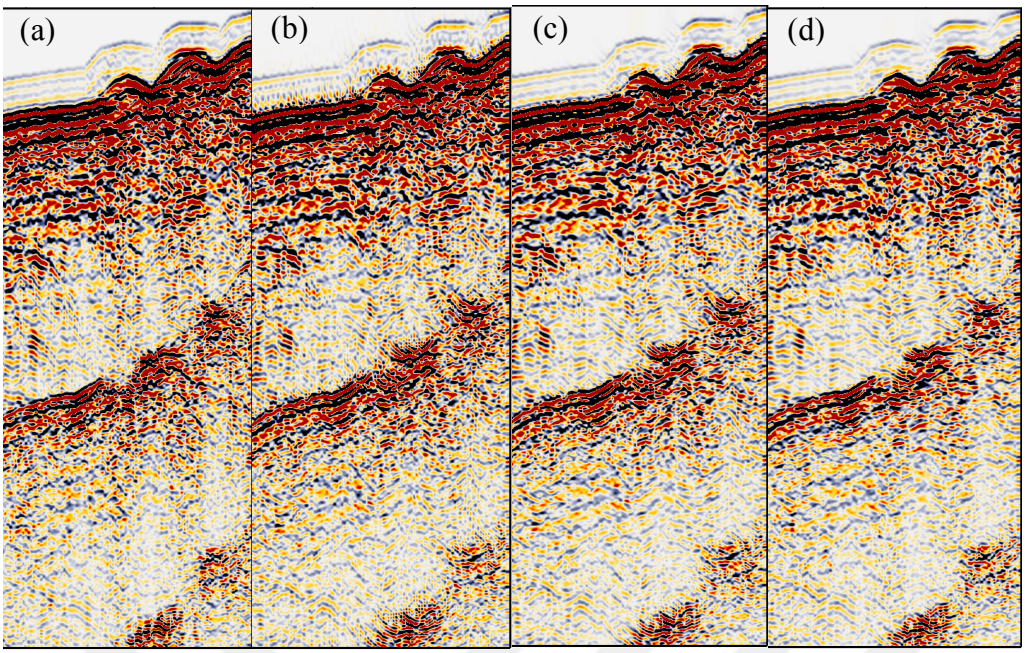

Figure 4.22 : Comparison of different TAU values with Velocity 01, (a) no migration, (b) Test 01, (c) Test 02 and (d) Test 03.

In general, as seen in Figure 4.22, the migration process widens the senclinals and contracts the anticlinals, however TAUs 2 ms and 12 ms introduces more artifacts which are particularly visible near the water bottom. With TAU=30 ms, the horizons are more continuous while the events are properly migrated as with smaller TAU values. The same TAU parameter is also tested with different velocities (Velocity 02) to see effect of different velocities which are presented in Figure 4.23.

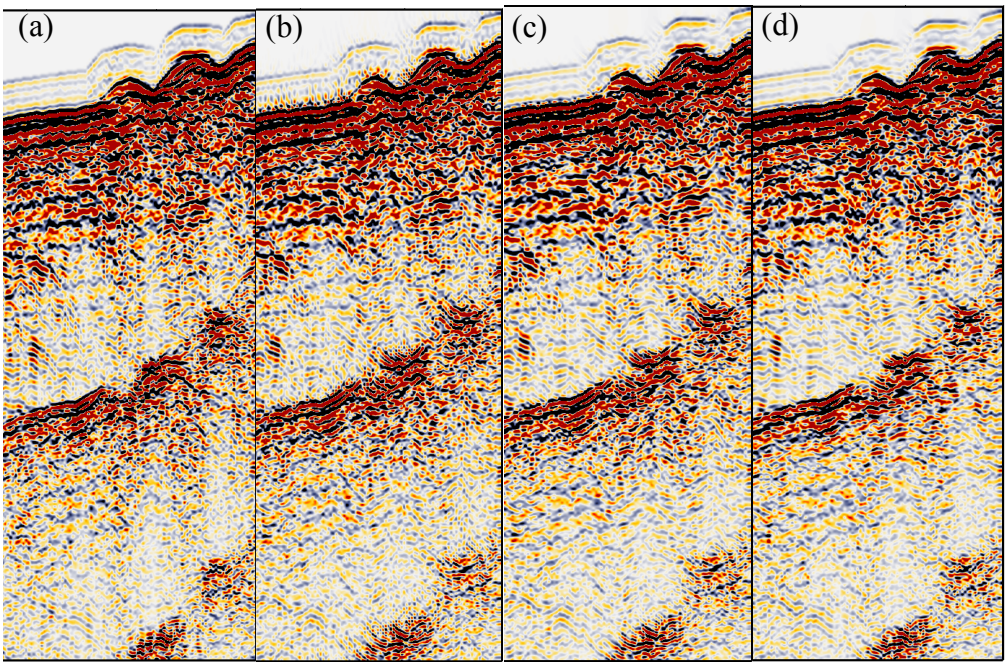

Figure 4.23 : Comparison of different TAU values with Velocity 02, (a) no migration, (b) Test 04, (c) Test 05 and (d) Test 06.

Again, the results in Figure 4.23 proves that higher TAU values around 30 ms is a good choice. As the last step of test, TAU=20 ms is used with different velocities; 03, 04 and 05, respectively, shown in Table 4.4. The differences are hardly recognizable however, linearly increasing velocity functions with relatively higher velocities as go deeper (Velocity 05) seem to work best.

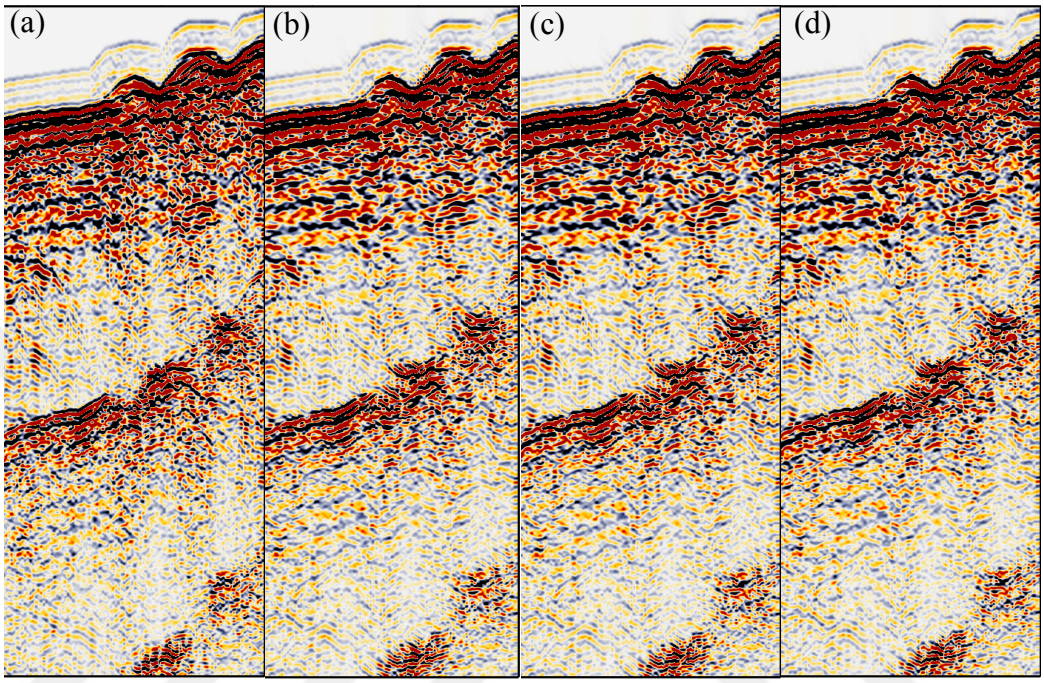

Figure 4.24 : Comparison of different velocities with TAU=20 ms values; (a) no migration, (b) Velocity 03, (c) Velocity 04 and (d) Velocity 05.

After fine-tuning the parameters in light of the test results, TAU=32 with Velocity 06 are used to produce final migrated sections.

4.6 Final Product

Processing of the seismic profiles were completed after carrying out all the processing steps explained above for all lines. In Figure 4.25, part of Line 9 (B9) raw data section and the final processed section are shown to emphasize the effectiveness of the data processing methods applied to the data.

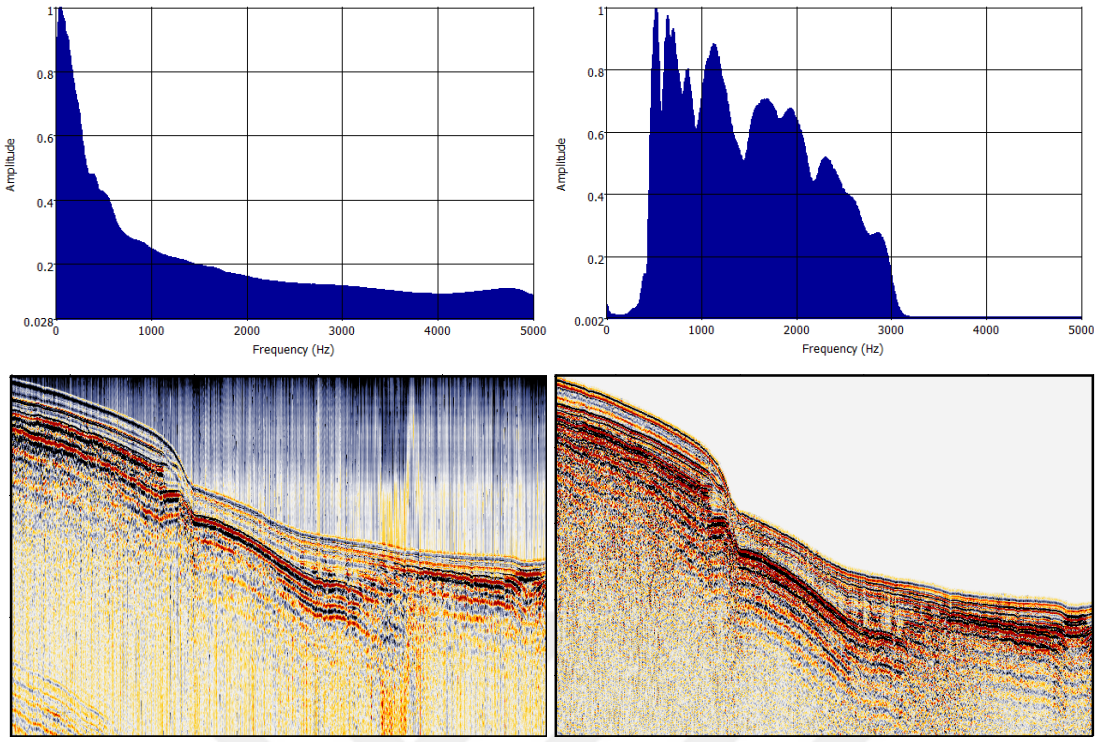

Figure 4.25 : Line 9 (B9) raw data (left) and processed data (right), amplitude spectra on top.

5. INTERPRETATION

In this chapter, following the data processing, the resulting sections of the "boomer" seismic reflection profiles acquired in Lake Sapanca in August 2018 in the scope of TÜBİTAK-1001 Scientific Research Project (Project No: 117Y130) are interpreted and presented.

Record length of the single-channel migrated sections are 150 ms and the interpretations are made on the full record length. However, definitive interpretation is confined mainly to the first 50-100 ms of the sections since the sections are contaminated with multiple reflection(s) below 100 ms and the penetration of the seismic energy from the source is limited by its frequency content which is very high for boomer sub-bottom profilers as mentioned in Chapter 3 – Method and Data Acquisition. Thus, the fault sticks are extended to the first multiple reflection with dashed lines. Interpreted sections are positioned such that the right side of the sections indicates S or SSE and the left side indicates N or NNE. Vertical axis of the sections shows two-way-travel time (TWT) in ms and horizontal axis shows the trace numbers either incrementing or decrementing from right to left, depending on the shooting direction of the lines. Since the data was acquired using a single receiver with 500-ms shot interval, the distance between each trace is approximately 1 m depending on the vessel speed. Vertical exaggeration of the sections is 1/25. For the calculation of the vertical exaggeration, a constant velocity of sound of 1500 m/s is used. Sections are presented in OpendTect seismic data interpretation software's "Seismics" colormap and VD (Variable Density) mode as this setting provided the most suitable visualization of the sections.

As the sections are analyzed, several faults are observed cutting through the lake bottom and the sediments. Sediment layers are parallel to the bottom of the lake with thicknesses ranging from approximately 3-6 m. According to Yalamaz (2016) and Gürbüz and Gürer (2008b), the sediments are sand-silt units in areas close to the shore, clay-containing units in the deeper parts, mud-containing units, and seismoturbidite units. In fact, for this study, line B9's location and direction were specifically chosen

to align with the locations of the core samples collected for Yalamaz (2002)'s study in order to compare the results.

As a general rule, the orientation of the seismic profiles was chosen so that they are perpendicular to the North Anatolian Fault which is thought to extend from east to west across the lake. In the scope of the same project, multibeam bathymetry data was also collected in the lake (Kurt et al., 2019). The resulting multibeam bathymetric map, which is created with 2-m grid spacing using GMT grdimage, along with the seismic profiles used in this thesis study overlaid on Lake Sapanca is shown in Figure 5.1. During the interpretation of the seismic profiles, the variations on the bathymetric image were also taken into consideration. In Figure 5.2, all processed seismic sections (pre-interpretation) in relation to one another and to the lake are shown in 3D perspective prepared using OpendTect software program. Additionally, the interpreted sections B11, B8, B5 and B1 are given in Figures 5.3, 5.4, 5.6 and 5.7, respectively.

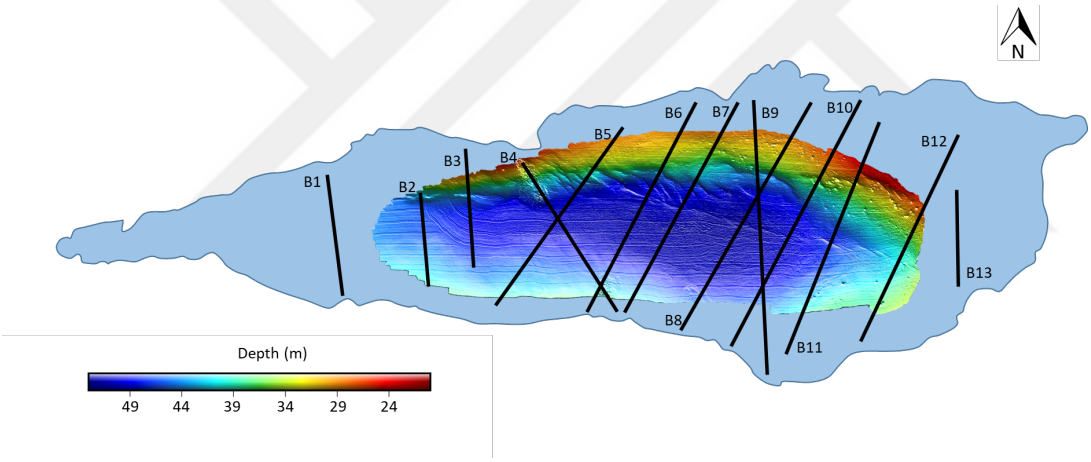

Figure 5.1 : Multibeam bathymetry map overlaid on Lake Sapanca along with the seismic reflection profiles. Bathymetry map is created with 2-m grid spacing using GMT grdimage with illumination direction of NE.

On section B11 located on the eastern part of the lake as shown in Figure 5.3, a vertical discontinuity creating a vertical trough on the lake bottom on the right side is visible in the area approximately in the middle of the section. This discontinuity which creates an approximately 1-1.5 m trough on its left side also affects the sediments in the deeper parts of the section. This structure is thought to belong to the northern strand of the North Anatolian Fault (NAF). Similar fault characteristics of line B11 located in the eastern part of the lake can also be observed on neighboring seismic sections of lines B12 and B10, which are 1 km east and 500 m west of B11, respectively (Figure 5.1 and Figure 5.2). On section B11, the sediments on the either side of the NAF show

different layering properties. Furthermore, in the south of the fault, at approximately 60 ms, it is observed that sedimentary package leans towards the fault with curvature whilst the sediments in the north of the fault show flat layering characteristics. This structure well coincides with the typical properties of strike-slip faults observed in seismic sections; the layering on either side of the fault are not aligned (Zalán, 1987). Not too far west to the study area, similar geometry of the northern strand of the NAF has also been identified in the seismic profiles acquired in Gulf of İzmit (Kurt and Yücesoy, 2008). Lineament extending from ESE towards WNW present in the multibeam bathymetric image can be associated with the discontinuity interpreted as the NAF on section B11 (Figure 5.1).

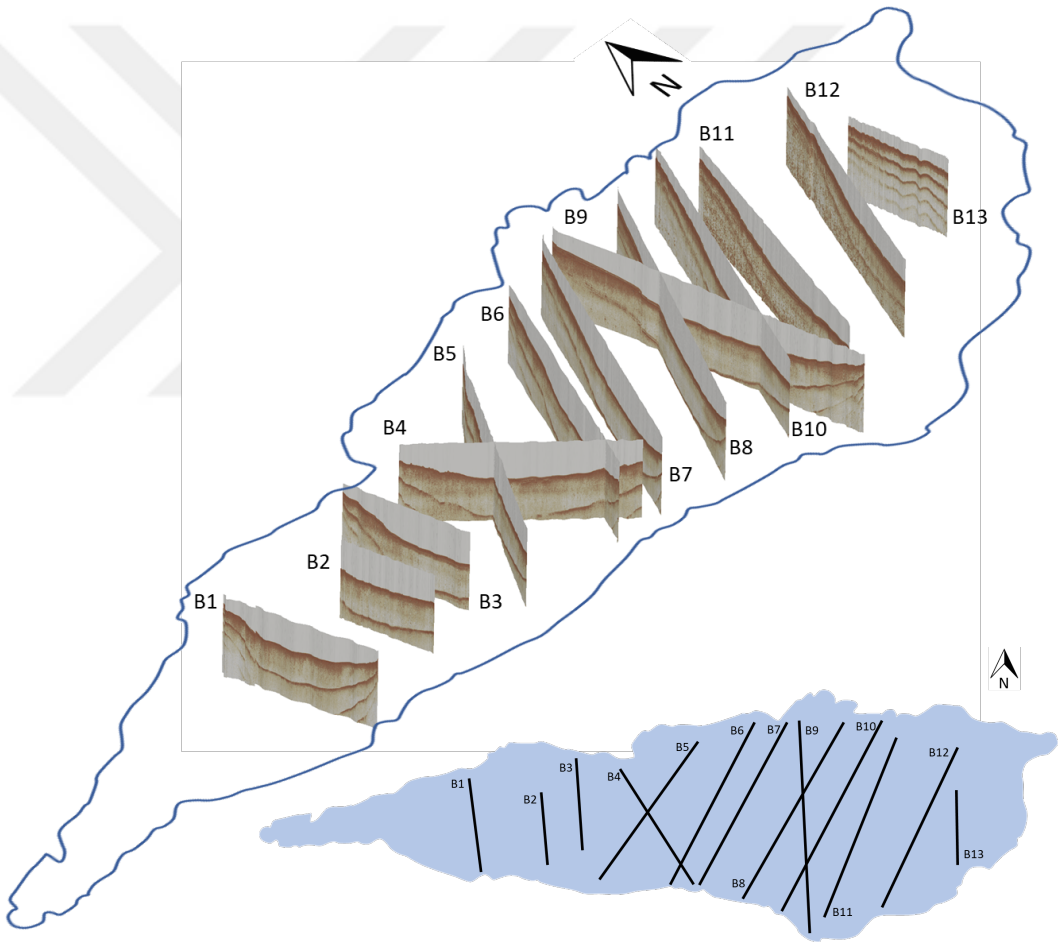

Figure 5.2 : Processed sections in their locations in relation to Lake Sapanca are shown as a fence diagram produced using open seismic interpretation software OpendTect. The bottom-right image shows boomer seismic reflection lines in map view.

Evidence of the discontinuity interpreted as the NAF on line B11 has also been examined on the profiles located towards the west of the lake. Hence, on the section B8 shown in Figure 5.4, the NAF is also observed as it forms unsimilar geometries on

the lake bottom and the sediments on either side of the fault. Here, the vertical trough on the lake bottom is less pronounced compared to the easterly lines, i.e. B10 and B11, however, the lineament on the multibeam bathymetric image can still be associated with this structure. Additionally, on section B8, at approximately 1200 m north of the NAF, a trough of 5 m is present and this shelf-like structure can also be associated with the small-scale bathymetric lineaments. This trough indicates secondary normal fault structures associated with the NAF. Another discontinuity, which is marked as "F1" in Figure 5.4, on the south part of line B8 can also be seen with similar mismatching effects on the sedimentation on either side. This strike-slip-fault-like structure's association with the bathymetric data is inconclusive, however, it might have some connection with the surface rupture mapped on land off the coast of Lake Sapanca in the south by Ambraseys and Zapotek (1969).

The fault map revealing the geometry of the faulting beneath Lake Sapanca is given in Figure 5.5. This map has been created by interpreting the seismic sections in conjunction with the multibeam bathymetric image of the lake. Sakarya and Sapanca segments shown on the map entering the lake in the east and leaving in the west, respectively, are from Lettis et al. (2002). 22 July 1967 Mudurnu Valley earthquake surface rupture (Ambreseys and Zapotek, 1969) is illustrated as in Dikbaş (2009). As seen on the fault map, the NAF extends from the east with WNW orientation making an approximately 30° angle with the map plane, then continues almost straight towards the west, starting from the location of line B5, until it leaves the lake. Note that some of the faults identified on the seismic sections are not illustrated on the fault map since their continuity on the adjacent sections is uncertain.

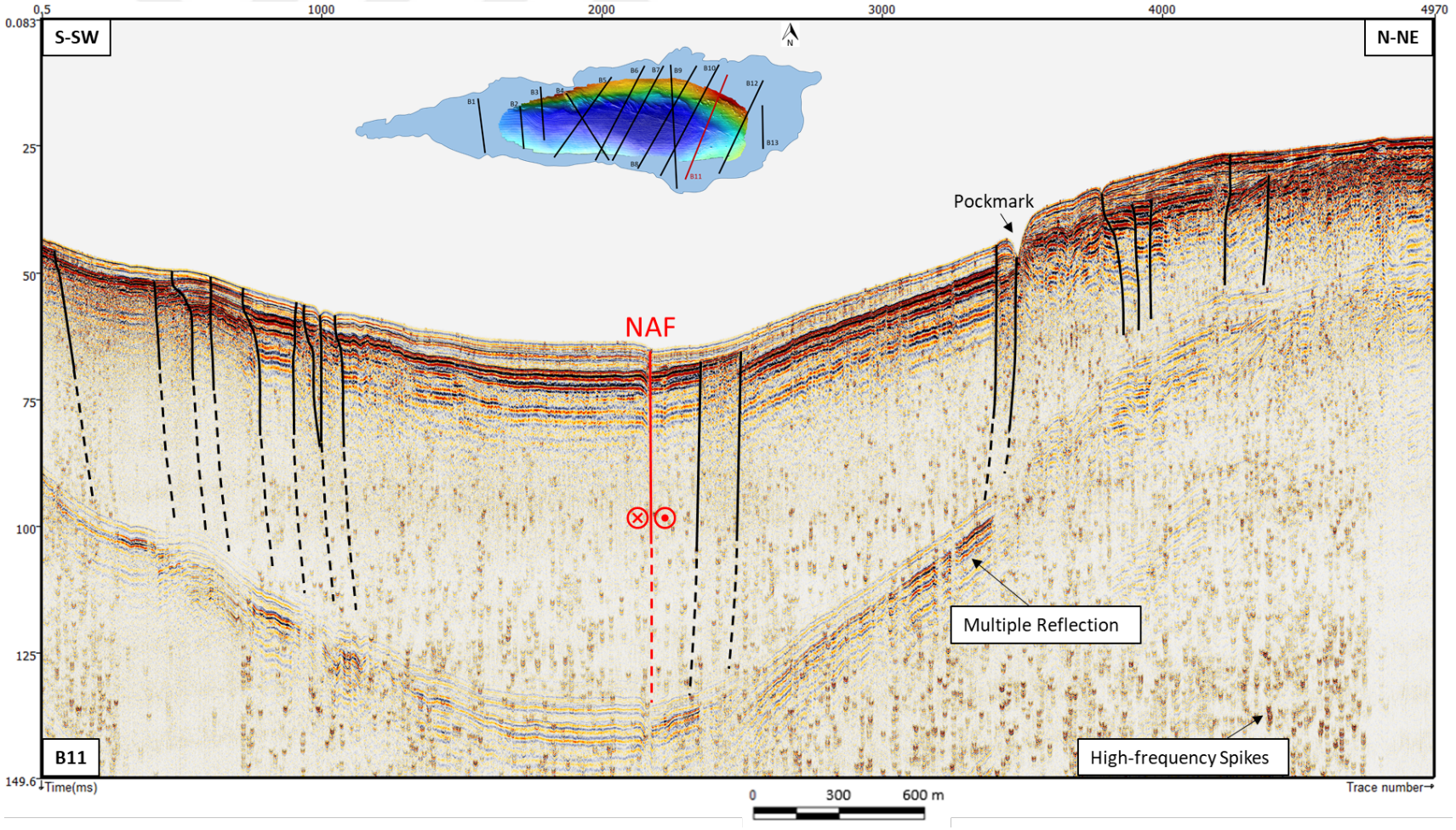

Figure 5.3 : Interpreted line B11. The North Anatolian Fault (NAF) is shown in red and all other faults shown in black. Vertical axis is two-way-travel time (TWT) in ms. Horizontal axis is trace number (distance between each trace is approximately 1 m). Vertical exaggeration is 25x (1/25).

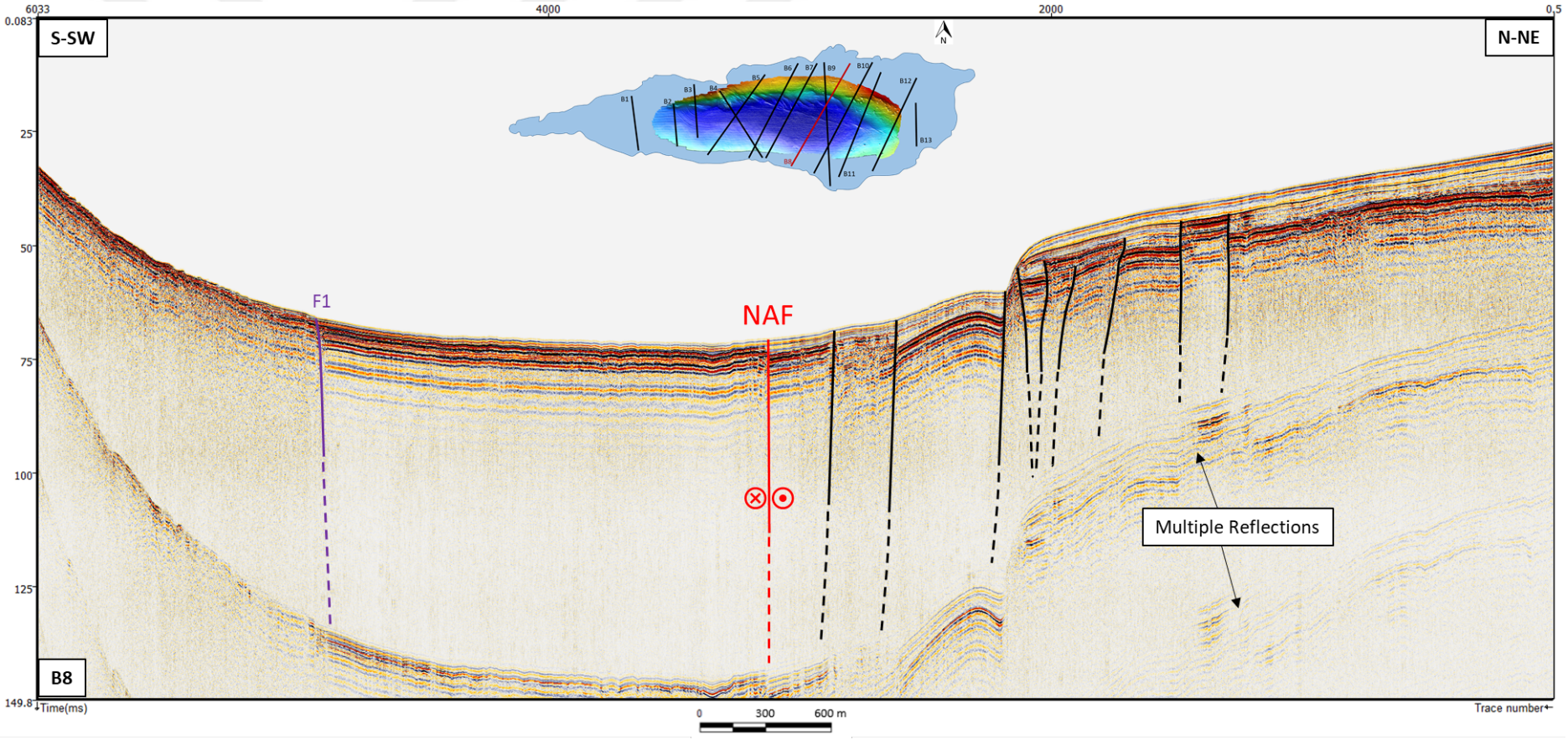

Figure 5.4 : Interpreted line B8. The North Anatolian Fault (NAF) is shown in red and all other faults shown in black and purple. Vertical axis is two-way-travel time (TWT) in ms. Horizontal axis is trace number (distance between each trace is approximately 1 m). Vertical exaggeration is 25x (1/25).

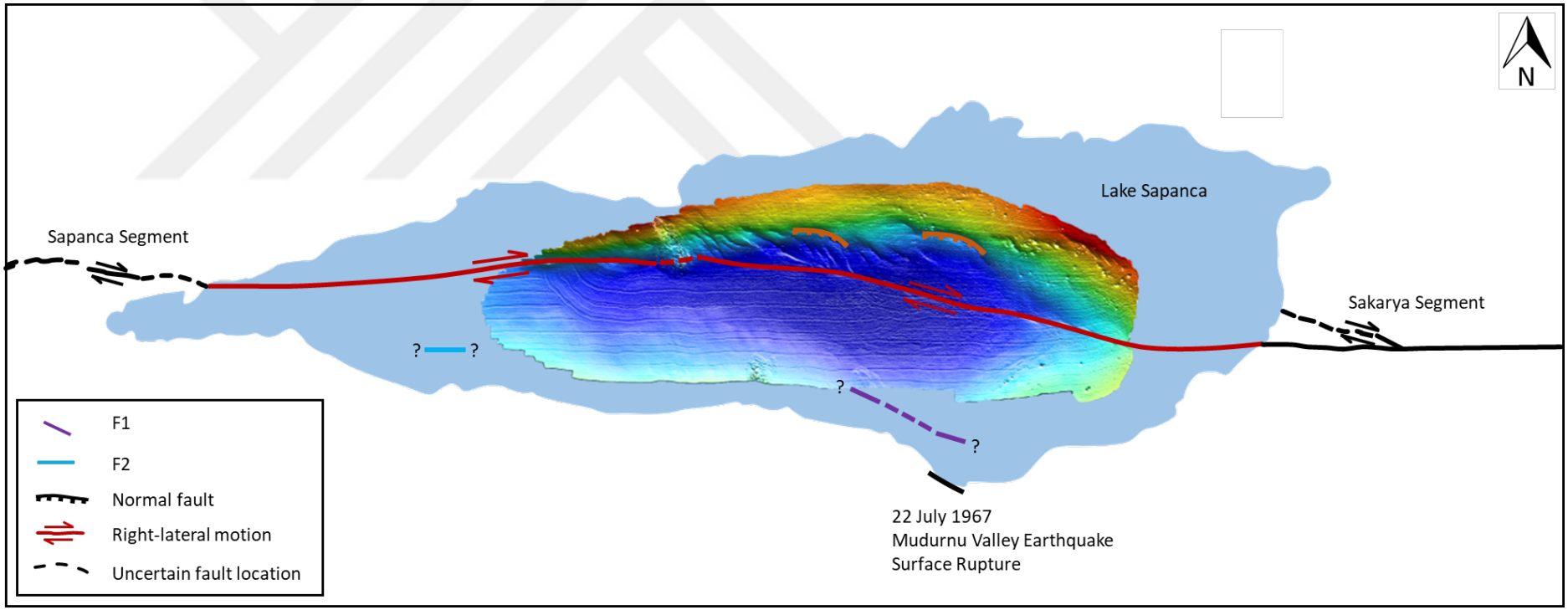

Figure 5.5 : Fault map derived from the interpreted seismic sections. The North Anatolian Fault (NAF) is shown in red. Sakarya and Sapanca fault segments on the east and west side of the lake are from Lettis et al. (2002). The NAF passing thorough the locations where there are no seismic profiles are illustrated based on Gülen et al. (2014). 22 July 1967 Mudurnu Valley earthquake surface rupture (Ambreseys and Zapotek 1969) is illustrated as in Dikbaş (2009).

Line B5 which is SSE NNW oriented and located in the middle part of the lake given in Figure 5.6. A vertical discontinuity similar to the one observed on lines B11 and B8 can also be seen on the mid-section of the line B5. This discontinuity also creates mismatching geometries in terms of layered sediments on either side of the discontinuity with less affected lake bottom geometry. Hence, the discontinuity seen on line B5 can also be associated with the NAF as it also coincides with the lineament on the bathymetric image. Series of step-like structures on the lake bottom with approximately 2-3 m elevation seen to the north of the NAF on section B5 can be associated to normal faulting. These faults to the north of the bathymetric image can be associated with the NW-SE orientated lineaments. Note that these structures are terminated as they reach the main fault, the NAF (Figure 5.5). Additional series of faults are also present on line B5 in the middle part of the section towards the south. The bathymetric data holds no significant trace regarding these group of faults therefore it cannot be directly associated. It is suspected that possible gas seeps through the cracks of these series of faults is very likely (Figure 5.6).

On the western-most line B1, the NAF can easily be identified on the bottom of the shelf on the northern part of the section although the line falls outside the multibeam bathymetry area (Figure 5.7). Furthermore, even without the existence of bathymetric data for the location where B1 lies, the NAF's location can be associated with easterly neighboring lines, i.e. B2 and B3, on which the NAF can also be identified in the north towards the shelf. On the south of the section, a discontinuity, which is marked as F2 in Figure 5.7, can be seen, however, this structure cannot be identified on sections B2 or B3. Thus, the nature or the origin of this strike-slip-fault-like structure is inconclusive. As observed in line B5, a more recurrent series of faulting is also present in the middle part of line B1. Again, no direct association to the bathymetry data can be mentioned. These faults can be making way for possible gas seepage through the cracks.

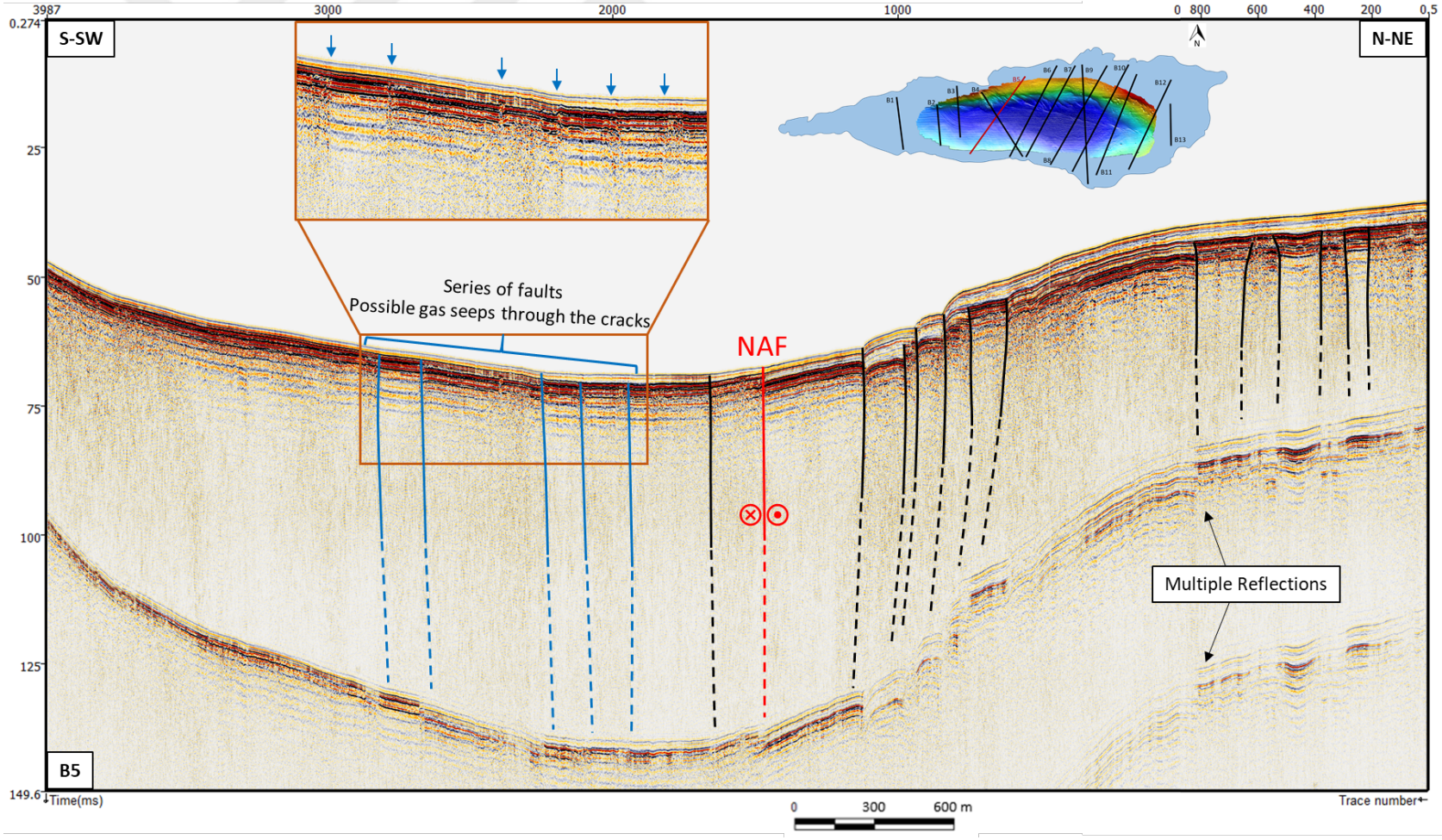

Figure 5.6 : Interpreted line B5. The North Anatolian Fault (NAF) is shown in red and all other faults shown in black and blue. Vertical axis is two-way-travel time (TWT) in ms. Horizontal axis is trace number (distance between each trace is approximately 1 m). Vertical exaggeration is 25x (1/25). Gas seeps are indicated with blue arrows in the zoomed-in image on the top-left.

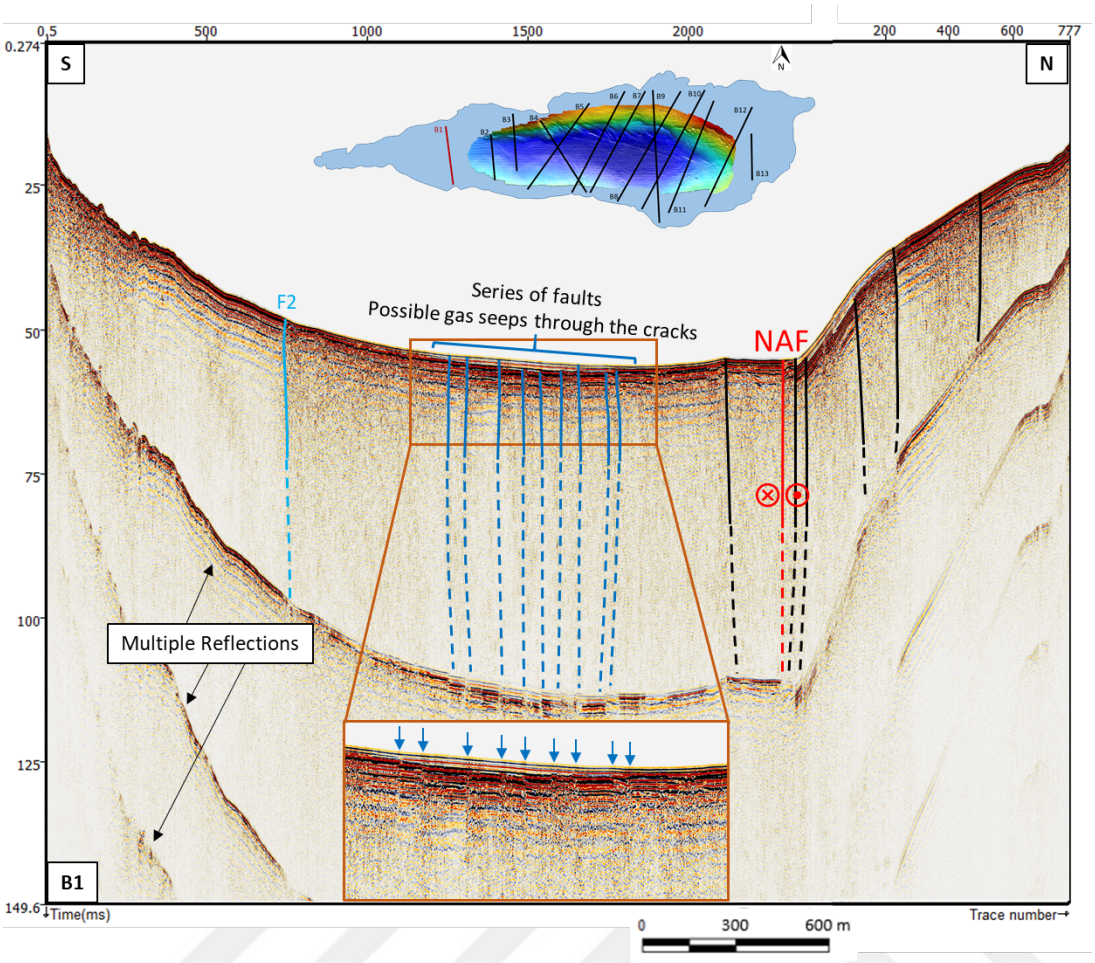

Figure 5.7 : Interpreted line B1. The North Anatolian Fault (NAF) is shown in red and all other faults shown in black and blue. Vertical axis is two-way-travel time (TWT) in ms. Horizontal axis is trace number (distance between each trace is approximately 1 m). Vertical exaggeration is 25x (1/25). Gas seeps are indicated with blue arrows in the zoomed-in image on the bottom.

As a result of the analysis and interpretation of all the sections from B1 to B13 in combination with the multibeam bathymetric image and previous studies, a fault map of Lake Sapanca showing the major active submarine tectonic structures has been produced as mentioned above and shown in Figure 5.5. In the previous studies, researchers speculate and agree that Lake Sapanca is a pull-apart basin and the NAF extends along the lake indicating a pull-apart and step-over geometry. On the contrary, with the close examination of the fault map produced in this study, it can be concluded that the NAF denotes a releasing bend geometry in Lake Sapanca.

6. CONCLUSIONS

In the last chapter of this thesis study, following conclusions can be derived based on the interpretation of the seismic sections and the analysis of the fault map produced according to the interpreted seismic sections.

In the migrated seismic sections, the North Anatolian Fault reveals itself as a vertical discontinuity creating a small-scale folding on the lake bottom as well as sedimentary misalignments as it extends deeper. This structure can be traced on most of the middle parts of the sections from B12 to B6 and on the northern part of the sections from B5 to B1 (Figure 5.2). All discontinuities interpreted as the NAF can also be associated with the lineaments observed on the multibeam bathymetric image.

On the fault map produced in this study, the NAF can be traced along Lake Sapanca entering from the south west corner of the lake and lengthening approximately 5 km towards the middle section of the lake with W-NW orientation making an approximately 30° angle to the map plane. Around where the line B5 is located, the fault slightly changes its direction towards the west as it continues almost straight for another 5 km until it leaves the lake at the north west corner. This fault geometry of the NAF indicates the fault has evolved with releasing bend characteristics in Lake Sapanca (Figure 5.5).

Strike-slip-fault-like discontinuity observed on the line B8 in the southern part of the lake might be associated with the 22 July 1967 Mudurnu Valley earthquake surface rupture.

The nature and the origin of another strike-slip-fault-like discontinuity seen on the line B1 is inconclusive due to no associations found on neighboring lines and also partly due to the lack of bathymetric data which could provide supportive evidence at the relevant location.

The series of recurrent small-scale faulting observed in the middle parts of the line B1 and B5 can be associated with gas seeps.

REFERENCES

Alpar B. and Yaltırak C. (2002). Characteristic features of the North Anatolian Fault in the eastern Marmara region and its tectonic evolution. *Marine Geology 190*, 329-350.

Ambraseys, N. N. and Zatopek, A. (1969). The Mudurnu valley, west Anatolia, Turkey, earthquake of 22 July 1967. *Bulletin of the Seismological Society of America*, *59*, 521- 589.

Armijo, R., Meyer, B., Hubert, A. and Barka, A. A. (1999). Westward propagation of the North Anatolian fault into the northern Aegean: timing and Kinematics. *Geology, 27,* 267–270.

Baltzer, A., Tessier, B., Nouzé, H., Bates, R., Moore, C. and Menier, D. (2005). Seistec seismic profiles: A tool to differentiate gas signatures. *Marine Geophysical Researches, 26*, 235–245.

Barka, A. A. (1992). The North Anatolian fault zone. *Annales Tectonicae, Spec. Iss. VI*, 164–195.

Barka, A. A., Akyüz, H. S., Altunel, E., Sural, G., Çakır, Z., Dikbaş, A., Yerli, B., Armijo, R., Meyer, B., de Chabalier, J.-B., Rockwell, T., Dolan, J. R., Hertleb, R., Dawson, T., Christofferson, S., Tucker, A., Fural, J., Langridge, R., Stenner, H., Lettis, W., Bachhuber, J. and Page, W. (2002). The surface rupture and slip distribution of the 17 August 1999 Izmit Earthquake (M7.4), North Anatolian Fault. *Bulletin of the Seismological Society of America, 92* (1), 43–60.

Bohnhoff, M., Harjes, H.-P. and Meier, T. (2005). Deformation and stress regimes at the Hellenic subduction zone from Focal Mechanisms. *Journal of Seismology 9* (3), 341–366.

Bohnhoff, M., Martínez-Garzón, P., Bulut, F., Stierle, E. and Ben-Zion, Y. (2016). Maximum earthquake magnitudes along different sections of the North Anatolian fault zone. *Tectonophysics, 674,* 147-165.

Bozkurt, E. (2001). Neotectonics of Turkey – a synthesis. *Geodinamica Acta*, *14*:1-3, 3-30.

Claerbout, J. F. and Johnson, A. G. (1971). Extrapolation of time dependent waveforms along their path of propagation. *Geophysics*, *26* (1-4), 285-294.

Claerbout, J. F. and Doherty, S. M. (1972). Downward continuation of moveout corrected seismograms. *Geophysics 37*, 741-768.

Dewey, F. and Şengör, A. M. C. (1979). Aegean and surrounding regions: complex multiple and continuum tectonics in a convergent zone. *Geological Society of America Bulletin, 90*, 84-92.

Dikbaş, A. (2009). *Kuzey Anadolu fay zonunun İzmit-Gölyaka (Düzce) arasındaki segmentlerin paleosismolojisi ve morfolojik özellikleri* (Doctoral dissertation). Istanbul Technical University, Eurasia Institute of Earth Sciences, ISTANBUL.

Dikbaş, A., Akyüz, H. S., Meghraoui, M., Ferry, M., Altunel, E., Zabcı, C., Langridge, R., Yalçıner, C. Ç. (2009). Paleoseismic history and slip rate along the Sapanca-Akyazı segment of the 1999 İzmit earthquake rupture (Mw=7.4) of the North Anatolian Fault (Turkey). *Tectonophysics 738–739*, 92–111.

Ekström, G., Nettles, M. and Dziewonski, A. M. (2012). The global CMT project 2004-2010: Centroid-moment tensors for 13,017 earthquakes. *Physics of the Earth and Planetary Interiors*, *200*, 1–9.

Emre, Ö., Awata, Y. and Duman, T. Y. (2003). 17 Ağustos 1999 İzmit Depremi Yüzey Kırığı. *Maden Tetkik ve Arama Genel Müdürlüğü, Özel Yayın Serisi, 1*, (ISBN:975-6595-53-1).

Flerit, F., Armijo, R., King, G. and Meyer, B. (2004). The mechanical interaction between the propagating North Anatolian Fault and the back-arc extension in the Aegean. *Earth and Planetary Science Letters, 224* (3(4)), 347–362.

Gülen L., Demirbağ E., Çağatay N., Utkucu M., Yıldırım E., Yalçın H. and Yalamaz, B. (2014). Sapanca Gölü'nün ayrıntılı batimetrisi, genç çökel istifi, aktif yapısal unsurları vasıtasıyla yakın bölgesinin sismojenik davranışının incelenmesi. Türkiye Ulusal Jeodezi ve Jeofizik Birliği (TUJJB) (Turkish National Union of Geodesy and Geophysics (TNUGG)). Proje No: TUJJB-UDP-03-10.

Gürbüz, A. and Gürer, Ö. (2008a). Anthropogenic affects on lake sedimentation process: a case study from Lake Sapanca, NW Turkey. *Environmental Geology, 56*, 299–307.

Gürbüz, A. and Gürer, Ö. (2008b). Tectonic geomorphology of the North Anatolian Fault Zone in the Lake Sapanca basin (Eastern Marmara Region, Turkey). *Geosciences Journal, 12* (3), 215-225.

Gürbüz, A., Suzanne, A. and Leroy, G. (2010). Science versus myth: was there a connection between the Marmara Sea and Lake Sapanca? *Journal of Quaternary Science, 25* (2), 103–114.

Jackson, J. A. and McKenzie, D. P. (1988). Rates of active deformation in the Aegean Sea and surrounding regions. *Basin Research*, *I*, 121- 128.

Kearey, P., Brooks, M. and Hill, I. (2002). *An Introduction to Geophysical Exploration.* Oxford (UK).: Blackwell Scientific.

Ketin, İ. (1948). Über die tektonisch-mechanischen Folgerungen aus den grossen anatolischen Erdbeben des letzten Dezenniums. *Geol. Rund., 36*, 77–83.

Ketin, İ. (1969). Kuzey Anadolu Fayı Hakkında. *Bull. Miner.Res. Explor. Inst. Turk., 76*, 1-25.

Kurt, H. and Yücesoy, E. (2008). Submarine structures in the Gulf of İzmit, based on multichannel seismic reflection and multibeam bathymetry. *Marine Geophysical Research, 30*, 73–84.

Kurt, H., Okut-Toksoy, N. G., İnanç, B., İşseven, T., Tün, M., Gönül, E. and Demirbağ, E. (2019). TÜBİTAK Scientific Research Project Development Report 1, Project No: 117Y130.

Koçyiğit, A. (1988). Tectonic setting of the Geyve Basin: Age and total displacement of the, Geyve Fault Zone. *METU J. Pure Appl. Sci., 21*, 81–104.

Kramer, F. S., Peterson, R. A. and Walter, W. C. (1969). Seismic Energy Sources. *Offshore Technology Conference,* Dallas, TX, 18-21 May (Handbook).

Lake. (n.d.). *Wikipedia.* Retreived Mar 30, 2019, from https://en.wikipedia.org/wiki/Lake

Lakes. (n.d.). Retreived Mar 30, 2019, from https://www.nationalgeographic.org/encyclopedia/lake/

Langridge, R. M., Stenner, H. D., Fumal, T. E., Christofferson, S. A., Rockwell, T. K., Hartleb, R. D., Bachhuber, J. and Barka, A. A. (2002). Geometry, slip distribution and kinematics of the surface rupture on the Sakarya fault segment during the 17 August 1999 İzmit, Turkey, Earthquake. *Bull. Seism. Soc. Amer.*, 92 (1), 107-125.

LePichon, X. L., Şengör, A. M. C., Kende, J., İmren, C., Henry, P., Grall, C. and Karabulut, H. (2015). Propagation of a strike slip plate boundary within an extensional environment: the westward propagation of the North Anatolian Fault. *Canadian Journal of Earth Sciences, 53*, (11): 1416-1439.

Lettis, W., Bachhuber, J., Witter, R., Brankman, C., Randolph, C. E., Barka, A. A., Page, W. D. and Kaya, A. (2008). Influence of releasing step-overs on surface fault rupture and fault segmentation: examples from the 17 August 1999 İzmit earthquake on the North Anatolian Fault, Turkey, *Bulletin of the Seismological Society of America, 92* (1), 19–42.

Li, Q.-Z. (2017). *High-Resolution Seismic Exploration.* Tulsa, OK.: Society of Exploration Geophysicists.

Marino, I. K., Santos, M. A. C. and Silva, C. G. (2013). Processing of high resolution, shallow seismic profiles, Guanabara Bay – Rio De Janeiro State, Brazil. *Brazilian Journal of Geophysics, 31* (4), 579-594.

McClusky, S., Balassanian, S., Barka, A. A., Demir, C., Ergintav, S., Georgiev, I., Gürkan, O., Hamburger, M., Hurst, K., Kahle, H., Kastens, K., Kekelidze, G., King, R., Kotzev, V., Lenk, O., Mahmoud, S., Mishin, A., Nadariya, M., Ouzounis, A., Paradissis, D., Peter, Y., Prilepin, M., Reilinger, R., Sanli, I., Seeger, H., Tealeb, A., Toksöz, M. N. and Veis, G. (2000). Global positioning system constraints on plate kinematics and dynamics in the eastern Mediterranean and Caucasus. *Journal of Geophysical Research, 105* (B3), 5695–5719.

McKenzie D. P. (1970). Plate tectonics of the Mediterranean region. *Nature, 220*, 239-343.

Oral M. B., Reilinger R. E., Toksoz M., Kong R. W., Barka A. A., Kınık I. and Lenk, O. (1995). Global positioning system offers evidence of plate motions in eastern Mediterranean. *EOS Transactions American Geophysical Union, 76* (2), 9-11.

Rahe, B., Ferrill, D. A. and Morris, A. P. (1998). Physical analog modeling of pull-apart basin evolution. *Tectonophysics, 285*, 21−40.

Ramsey, P. (2017). Sub-bottom Profiling Acquisition Techniques in HYPACK®. Retrieved March 20, 2019, from http://www.hypack.com/File%20Library/Resource%20Library/Technical%20Notes/Sub-bottom-Profiling-Acquisition-Techniques-in-HYPACK.pdf

Reilinger, R., McClusky, S., Vernant, P., Lawrence, S., Ergintav, S., Çakmak, R., Özener, H., Kadirov, F., Guliev, I., Stepanyan, R., Nadariya, M., Hahubia, G., Mahmoud, S., Sakr, K., ArRajehi, A., Paradissis, D., Al-Aydrus, A., Prilepin, M., Guseva, T., Evren, E., Dmitrotsa, A., Filikov, S. V., Gomez, F., Al-Ghazzi, R. and Karam, G. (2006). GPS constraints on continental deformation in the Africa– Arabia–Eurasia continental collision zone and implications for the dynamics of plate interactions. *Journal of Geophysical Research, 111*, B05411.

Rotstein Y. (1984). Counterclockwise rotation of Anatolian block. *Tectonophysics, I08*, 71-9 1.

Seber D., Vallve M., Sando, E., Steer D. and Barazangi M. (1997). Middle, East tectonics: applications of Geographic Information Systems (GIS). *GSA Today, 7*, 1-6.

Sengburg, R. L. (1983). *Seismic Exploration Methods.* Boston, MA.: IHRDC.

Simpkin, P. G. (2005). The Boomer sound source as a tool for shallow water geophysical exploration. *Marine Geophysical Researches***,** *26,* 171-181.

Stoker, M. S., Pheasant, J. B. and Josenhans, H. (1997). *Seismic methods and interpretation (Glaciated Continental Margins: An Atlas of Acoustic Images)*. London (UK).: Chapman and Hall.

Straub, C., Kahle, H.-G. and Schindler, C. (1997). GPS and geologic estimates of the tectonic activity in the Marmara Sea region, NW Anatolia. *Journal of Geophysical Research, 102* (B12), 27587–27601.

Şaroğlu, F. (1988). Age and pure offset of the North Anatolian Fault. *J. Pure Appl. Sci., 21*, 65-79.

Şengör A. M. C. and Yılmaz, Y. (1981). Tethyan evolution of Turkey: A plate tectonic approach. *Tectonophysics, 75*, 181–241.

Şengör A. M. C., Görür, N. and Şaroğlu, F. (1985). Strike-slip faulting and related basin formation in zones of tectonic escape: Turkey as a case study, in: Biddle K.T., Christie-Slick N. (eds.), Strike-slip Faulting and Basin Formation. *Soc. Econ. Paleontol. Mineral. Sp. Pub., 37*, 227-264.

Şengör A. M. C., Tüysüz, O., İmren, C., Sakınç, M., Eyidoğan, H., Görür, N., LePichon, X. and Rangin, C. (2005). The North Anatolian Fault: a new look. *Annual Review of Earth and Planetary Sciences, 33*, 37–112.

Toksöz, M. N., Shakal, A. F., Michael, A. J. (1979). Space-time migration of earthquakes along the North Anatolian fault zone and microseismic gaps. *Pure Appl. Geophys. 117* (19), 1258-1270.

Tóth T. (2011). Single and Multichannel Seismics. In: Gupta H.K. (eds) Encyclopedia of Solid Earth Geophysics. Encyclopedia of Earth Sciences Series. Springer, Dordrecht.

Wail, A. M. and Al-Shuhail, A. A. (2011). *Processing of Seismic Reflection Data Using MATLAB™*.: Morgan & Claypool Publishers.

Westaway R. (1994). Present-day kinematics of the Middle East and Eastern Mediterranean. *Journal of Geophysical Research, 99*, 12071-12090.

Yalamaz, B. (2016). *Sapanca Gölü Çökellerinde Deprem Kaynaklı Kütle Akması Birimlerinin Belirlenmesi ve Tarihi Depremlerle Eşleştirilmesi* (Master's thesis). Istanbul Technical University, Graduate School of Science Engineering and Technology, ISTANBUL.

Yılmaz, Ö. (2001). *Seismic Data Analysis.* Tulsa, OK.: Society of Exploration Geophysicists.

Zalán, P. (1987). Identification of strike-slip faults in Seismic section. Proc. Am. Assoc. Pet. Geol. Annu. Meet., 1988. 10.1190/1.1892142.

CURRICULUM VITAE

Name Surname **: Gökçe İregör**

Place and Date of Birth **: Ordu, 26 April 1980**

E-Mail **: sensoyg@yahoo.com**

EDUCATION **:**

- **B.Sc.** **:** 2004, Istanbul Technical University, Faculty of Mines, Geophysical Engineering Department

PROFESSIONAL EXPERIENCE AND REWARDS:

- 2001-2004 Istanbul Technical University Faculty of Mines Computer Laboratory – Student employee as an Assistant Computer Administrator.
- 2008-Present PGS Geophysical (Norway) – Offshore Operations – Chief Geophysicist.